

AD-A285 865



SMC-TR-94-39

AEROSPACE REPORT NO.
TR-93(3505)-1

①

LADAR Detection Statistics in the Presence of Pointing Errors

15 December 1993

Prepared by

H. T. YURA
Electronics Technology Center
Technology Operations

Prepared for

SPACE AND MISSILE SYSTEMS CENTER
AIR FORCE MATERIEL COMMAND
2430 E. El Segundo Boulevard
Los Angeles Air Force Base, CA 90245

6998

94-34139



2

Development Group

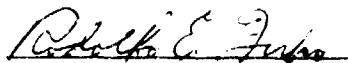
APPROVED FOR PUBLIC RELEASE
DISTRIBUTION UNLIMITED

 **THE AEROSPACE
CORPORATION**
El Segundo, California

This report was submitted by The Aerospace Corporation, El Segundo, CA 90245-4691, under Contract No. F04701-88-C-0089 with the Space and Missile Systems Center, 2430 E. El Segundo Blvd., Los Angeles Air Force Base, CA 90245. It was reviewed and approved for The Aerospace Corporation by T. A. Galantowicz, Principal Director, Electronics Technology Center.

This report has been reviewed by the Public Affairs Office (PAS) and is releasable to the National Technical Information Service (NTIS). At NTIS, it will be available to the general public, including foreign nationals.

This technical report has been reviewed and is approved for publication. Publication of this report does not constitute Air Force approval of the report's findings or conclusions. It is published only for the exchange and stimulation of ideas.


R. FIRPO, Major, USAF
SMC/XRF

REPORT DOCUMENTATION PAGE			Form Approved OMB No. 0704-0188	
<small>Public reporting burden for this collection of information is estimated to average 1 hour per response, including the time for reviewing instructions, searching existing data sources, gathering and maintaining the data needed, and completing and reviewing the collection of information. Send comments regarding this burden estimate or any other aspect of this collection of information, including suggestions for reducing this burden to Washington Headquarters Services, Directorate for Information Operations and Reports, 1215 Jefferson Davis Highway, Suite 1204, Arlington, VA 22202-4302, and to the Office of Management and Budget, Paperwork Reduction Project (0704-0188), Washington, DC 20503.</small>				
1 AGENCY USE ONLY (Leave blank)	2 REPORT DATE 15 December 1993	3 REPORT TYPE AND DATES COVERED		
4 TITLE AND SUBTITLE LADAR Detection Statistics in the Presence of Pointing Errors		5 FUNDING NUMBERS F04701-88-C-0089		
6 AUTHOR(S) Yura, Hal T.				
7 PERFORMING ORGANIZATION NAME(S) AND ADDRESS(ES) The Aerospace Corporation Technology Operations El Segundo, CA 90245-4691		8 PERFORMING ORGANIZATION REPORT NUMBER TR-93(3505)-1		
9 SPONSORING/MONITORING AGENCY NAME(S) AND ADDRESS(ES) Space and Missile Systems Center Los Angeles Air Force Base Los Angeles, CA 90009-2960		10 SPONSORING/MONITORING AGENCY REPORT NUMBER SMC TR 94-39		
11 SUPPLEMENTARY NOTES				
12a DISTRIBUTION/AVAILABILITY STATEMENT Approved for public release; distribution unlimited			12b DISTRIBUTION CODE	
13 ABSTRACT (Maximum 200 words) <p>The probability of detection of optically rough targets by pulsed LADAR systems that employ direct detection is considered here. It is assumed that the LADAR operates under conditions of both unintentional pointing off-set bias (i.e., bore-sight error) and jitter. Under these conditions, the probability of detection of targets in both the near and far field of the collecting aperture (i.e., for resolved, partially resolved, and unresolved targets) and for both large and small photoelectron counts is derived, and, in many cases of practical interest, accurate, elementary analytic approximations that are useful for parametric system studies are obtained. As such, the approximate engineering expressions derived here will be useful, for example, to those performing engineering modeling of space-based LADAR systems. A number of appendices are included to serve as technical references, where some key results employed in the main body of the report are derived. In particular, an interesting new mathematical result involving the complementary incomplete gamma function and an analytic expression for the probability distribution function of a signal photocount obeying Bose-Einstein statistics (such as that arising from unresolved targets) immersed in Poisson noise are derived.</p>				
14 SUBJECT TERMS Optical Radar, Detection Statistics, LADAR, Statistical Optics, Pointing Errors			15 NUMBER OF PAGES 70	
			16 PRICE CODE	
17 SECURITY CLASSIFICATION OF REPORT UNCLASSIFIED	18 SECURITY CLASSIFICATION OF THIS PAGE UNCLASSIFIED	19 SECURITY CLASSIFICATION OF ABSTRACT UNCLASSIFIED	20 LIMITATION OF ABSTRACT	

Contents

Preface	vii
Introduction	1
Probability of Detection for Low Photoelectron Counts	13
Detection Statistics without Pointing Errors	13
Detection Statistics with Pointing Errors	15
Probability of Detection for High Photoelectron Counts	23
Detection Statistics without Pointing Errors	25
Detection Statistics with Pointing Errors	31
Summary	41
References	45

Appendixes

A	Pointing-error Statistics	A-1
B	The Negative-binomial Distribution: Some Limiting Cases	B-1
C	Signal-noise-limited Detection Statistics	C-1
D	Probability Distribution of a Signal Photoelectron Count Obeying Bose-Einstein Statistics Immersed in Poisson Noise	D-1

Figures

1.	The parameter m , the mean number of speckles contained within the collection aperture, for a wavelength of 0.532 microns and a collecting aperture diameter of 0.2 m	6
2.	The mean number of signal photocounts as a function of range for various values of laser beam divergence	8
3.	The mean number of signal photocounts as a function of range for various values of the laser spot area at the target	9

Figures (Cont'd)

4.	Probability of detection for the case where $m = 1.5$ and $b = 0$	18
5.	Probability of detection for the case where $m = 1.5$ and $b = 0.5$	19
6.	Probability of detection for the case where $m = 1.5$ and $b = 1$	20
7.	Probability of detection for the case where $m = 15$ and $b = 0$	21
8.	Probability of detection for the case where $m = 15$ and $b = 0.5$	22
9.	Probability of detection for the case where $m = 15$ and $b = 1$	23
10.	Probability of detection for a large number of photocounts and m is large ($\geq 5-10$) and $b = 0$	33
11.	Probability of detection for a large number of photocounts and m is large ($\geq 5-10$) and $b = 0.5$	34
12.	Probability of detection for a large number of photocounts and m is large ($\geq 5-10$) and $b = 1$	35
13.	Probability of detection for $m = 1$, $b = 0$ and both the SNR and TNR are large.....	38
14.	Probability of detection for $m = 1$, $b = 0.5$ and both the SNR and TNR are large.....	39
15.	Probability of detection for $m = 1$, $b = 1$ and both the SNR and TNR are large.....	40
C-1.	Signal-noise-limited detection: a comparison of the detection probability as a function of the signal-to-threshold ratio.....	C-4
D-1.	Probability density of a signal obeying Bose-Einstein statistics immersed in Poisson noise, where the mean signal count = 1 for various values of the noise count	D-3
D-2.	Probability density of a signal obeying Bose-Einstein statistics immersed in Poisson noise, where the mean signal count = 10 for various values of the noise count	D-3
D-3.	Probability density of a signal obeying Bose-Einstein statistics immersed in Poisson noise, where the mean signal count = 100 for various values of the noise count	D-4
D-4.	Probability density of a signal obeying Bose-Einstein statistics immersed in Poisson noise, where the mean signal count = 1000 for various values of the noise count	D-4
D-5.	Quantity $G(K, n) = \Gamma(K + 1, n) / \Gamma(K + 1)$ for photocounts near 1000 and various values of n	D-5

Tables

1.	Definitions of Some Key Parameters and Reference to their Appearance in the Body of this Paper.....	43
2.	Probability of Detection per Pulse, Averaged Over the Pointing Statistics in the High Photoelectron Count Regime	44

A-1

Preface

I would like to thank S. A. Cantor for bringing this problem to my attention and S. C. Moss for his helpful comments and continual encouragement during the course of this work.

Introduction

The acronym LADAR is used here to distinguish optical radar systems that are used to detect and range hard-body targets from LIDAR systems that detect scattered laser light from various diffuse molecular and particulate constituents in the atmosphere. Here we consider a direct-detection (monostatic) LADAR system that emits a burst of short (~ 10 to 20 ns Q-switched) laser pulses. These pulses are assumed to reflect off a diffuse target and are subsequently collected by the LADAR, and a range determination of the target is obtained. Since the forms available in the literature for the detection probability per pulse are often untenable for practical systems studies, it is of particular concern here to obtain elementary analytic approximations to the probabilities of detection in various circumstances that are suitable for use in commercially available spreadsheet programs (e.g., EXCEL, JAVELIN, or 123). Although the primary purpose of this report is to obtain results for the probability of detection per pulse, we also present an example of a target detection algorithm, constructed from multiple pulse statistics, which can be used to increase the overall detection probability when the probability of detection per pulse, P_d , is low.

We consider targets that can be both in the near and far field of the receiving aperture and LADAR systems operating in the small and large photocount regime. Here we assume for precision that the laser beam spot size at the target is large in comparison to the size of the target (i.e., the transmitted beam does not resolve the target) and the target depth (in the range direction) is small in comparison to the (longitudinal) coherence length of the transmitted beam. When light, having a deterministic variation over space and time (e.g., specular reflection from a corner cube or a glint), impinges on a (square-law) photodetector it can be shown that the resulting photoelectron counts obey Poisson

statistics. That is, we assume here that the probability of observing K photoevents over a time period that is long compared to the optical period is given by

$$P(K) = \frac{K_s^K}{K!} e^{-K_s}, \quad K = 0, 1, 2, \dots, \quad (1)$$

where K_s is the mean number of photoevents expected per pulse.¹ This quantity is given by

$$K_s = \left(\frac{\eta}{h\nu} \right) E_s, \quad (2)$$

where E_s is the mean return integrated signal fluence per pulse (i.e., collected return energy per pulse), h is Planck's constant, ν is the optical frequency, and η is the detector quantum efficiency. An explicit expression for E_s is obtained from the LADAR range equation for a diffuse Lambertian target and a LADAR system with no boresight error or jitter:²

$$E_s = \left(\frac{E_t}{A_{\text{spot}}} \right) \left(\frac{\rho A_T}{\pi} \right) \left(\frac{A_R}{R^2} \right) T^2, \quad (3)$$

where

E_t = Transmitted laser energy per pulse

A_{spot} = Equivalent laser beam spot area at the target

ρ = Diffuse target reflectance

A_T = Target area, normal to the line-of-sight

R = Propagation range

A_R = Receiver clear-aperture area

T = One-way propagation path transmittance

For propagation through vacuum, T is just the LADAR system optics transmittance. Here, we assume a laser beam irradiance profile given by

$$I(\theta) = I_0 \exp\left[-\theta^2/2\theta_0^2\right] \quad , \quad (4)$$

where I_0 is the beam irradiance for $\theta = 0$. For systems that employ a fixed beam divergence, we thus have

$$A_{\text{spot}} = 2\pi(R\theta_0)^2 \quad (5)$$

We note that the $1/\sqrt{e}$ full-angle beam divergence is equal to $2\theta_0$, and the corresponding $1/e^2$ full-angle beam divergence equals $2(2\theta_0) = 4\theta_0$. Thus, for example, a beam characterized here by $\theta_0 = 5\mu\text{rad}$ corresponds to a beam with a $20\mu\text{rad}$ $1/e^2$ full-angle beam divergence. Such a system results in energy returns that are proportional to R^{-4} . On the other hand, LADAR systems employing appropriate zoom optics that keep $A_{\text{spot}} =$ constant at the target, independent of range, result in energy returns proportional to R^{-2} . Here we assume uniformly illuminated targets for simplicity. The case of nonuniformly illuminated targets can be formally included by replacing A_T in the LADAR range equation by some effective target area $(A_T)_{\text{eff}} (\leq A_T)$. For example, for a target possessing a circular cross-sectional area normal to the line-of-sight and a LADAR employing a laser beam spread of Gaussian shape, it can be shown that $(A_T)_{\text{eff}} = \pi r_T^2 f$, where the reduction factor $f = (2\theta_0^2/\theta_T^2) \left[1 - e^{-\theta_T^2/2\theta_0^2}\right]$, r_T is the radius of the target, $\theta_T = r_T/R$, and θ_0 is the $1/\sqrt{e}$ angular laser beam radius. Uniform illumination is obtained for $\theta_T \ll \theta_0$, where $f = 1$ and $(A_T)_{\text{eff}} = A_T$. Although very few optical radar transmitters resolve the target, this case can be incorporated into the present analysis simply by setting $A_T = A_{\text{spot}}$ in Eq. (3).

In many cases of practical concern, the return signal is not deterministic, but rather has a random variation over space and time (e.g., from pulse to pulse). It is now necessary to treat the Poisson distribution of Eq. (1) as a conditional probability distribution, the conditioning being based on knowledge of the probability distribution of the return integrated (over the receiver collecting aperture) signal fluence. In practice, however, it is the unconditional probability distribution of photocounts that relates to required system performance quantities such as the probability of detection. The unconditional probability distribution is obtained by averaging the conditional Poisson distribution of Eq. (1) over the statistics of the return integrated signal fluence. The details of the calculation have been documented in Reference (3) with the result that

$$P(K) = \frac{\Gamma(K+m)}{\Gamma(K+1)\Gamma(m)} \left[1 + \frac{m}{K_s}\right]^{-K} \left[1 + \frac{K_s}{m}\right]^m, \quad (6a)$$

$$E[K] = K_s, \quad (6b)$$

$$\text{Var}[K] = K_s + \frac{K_s^2}{m}, \quad (6c)$$

where $E[\cdot]$ and $\text{Var}[\cdot]$ denote the expectation value and variance, respectively, $\Gamma(\cdot)$ is the gamma function, and m is given by

$$m \cong 1 + \frac{A_R A_T}{\lambda^2 R^2} \quad (7)$$

The first and second term on the right-hand side of Eq. (6c) is the signal shot-noise and speckle-noise contribution to the signal variance, respectively. As discussed in Reference

(3), m can be interpreted as the mean number of independent irradiance correlation cells (i.e., speckles) contained within the collecting aperture. Examination of Eq. (6) reveals that the signal statistics depend not only on the mean-signal photoelectron count per pulse, K_s , but, in addition, also on the mean number of correlation cells, m , (or speckles) contained within the collecting aperture. Since the signal-count fluctuations increase with decreasing values of m , it is seen that LADAR system performance generally deteriorates as the number of speckles decreases with the worst performance obtained for $m = 1$.⁴ In addition, it is easily seen from Eq. (6) that the Poisson distribution is an accurate approximation to the negative-binomial when $m \gg K_s$. Thus, for an optically rough target, the assumption of Poisson signal statistics is justified only when the average number of signal photoelectrons per spatial correlation cell is much less than unity. For any given physical situation, both K_s and m are obtained from Eqs. (2) and (7), and the results are used in Eq. (6).

The distribution given by Eq. (6) is known as the negative-binomial distribution. For m near unity (unresolved targets), a single speckle is contained in the collecting aperture, the collected energy obeys negative-exponential statistics, and the corresponding photocounts obey Bose-Einstein statistics. On the other hand, for $m \gg 1$ (resolved targets), many speckles are contained within the collecting aperture, and the collected energy distribution behaves as a delta function centered at the mean value E_s . Hence, in the limit $m \rightarrow \infty$, $P(K)$ must obey Poisson statistics. These analytic features are contained in the negative-binomial distribution given by Eq. (6).

Figure 1 is a plot of m as a function of range for a wavelength of $0.532\mu\text{m}$ and a collecting-aperture diameter of 20 cm. Examination of Figure 1 reveals that for $R \geq 1.5$ Megameters, $m \sim 1$ for $A_T \geq 1 \text{ m}^2$. As a result, the return-signal photocount is well

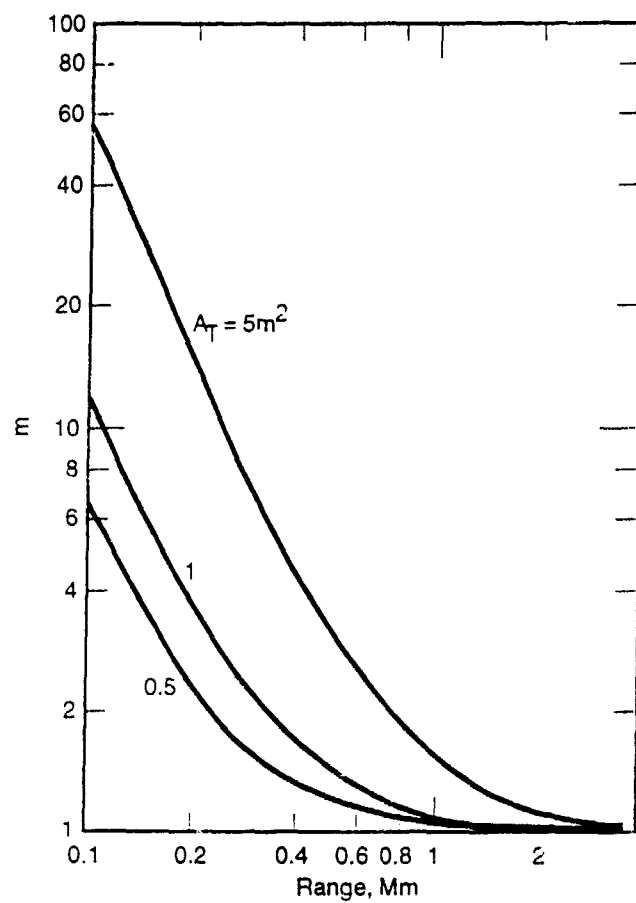


Figure 1. The parameter m , the mean number of speckles contained within the collection aperture, for a wavelength of 0.532 microns and a collecting aperture diameter of 0.2 m.

approximated by Bose-Einstein statistics. On the other hand, for $R \leq 0.5$ Mm, $m \gg 1$ for $A_T \geq 5$ m² and hence the signal photocount is well approximated by Poisson statistics if $K_s \ll m$.

We now distinguish between the low signal photoelectron count regime, where $K_s \ll 100$, and the high-count regime, where $K_s \geq 100$. In the low photocount regime, the discrete character of the signal counts is retained while for the high photocount regime it is customary to characterize the collected signal by a continuous distribution of signal current i , related to the corresponding signal photocount by

$$i = \frac{qK}{\tau} \quad (8)$$

where q is the electronic charge, and τ is the reflected return laser signal pulse width.

As an example illustrating the expected value of signal counts per pulse obtained under various circumstances, we consider the following values of LADAR system parameters: $E_T = 0.5$ J/pulse, a collector diameter of 20 cm, $T^2 = 0.5$, $\lambda = 0.532\mu\text{m}$, $A_T = 5$ m², $\rho = 0.4$, and $\eta = 0.8$. We consider a system that employs a fixed laser beam width as well as one that keeps a fixed spot at the target, independent of range. The results for K_s as obtained from Eq. (2) are plotted in Figures 2 and 3 as a function of range for various values of θ_0 and A_{spot} , respectively. Examination of Figure 2 reveals that, for the parameters assumed above, the low photoelectron-count regime ($K_s \ll 100$) is expected for $R \geq 0.4 - 1.3$ Mm, depending on the value of θ_0 for the fixed-beam-divergence system. On the other hand, examination of Figure 3 reveals that for the fixed-spot-on-target case the corresponding low photocount regime is expected for $R \geq 1.0 - 3$ Mm.

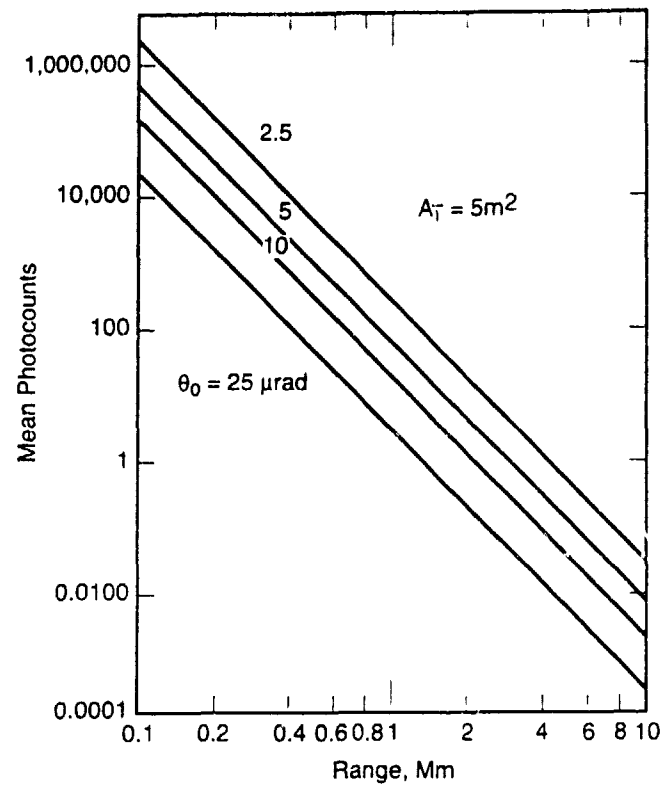


Figure 2. The mean number of signal photocounts as a function of range for various values of laser beam divergence. Note that the beam angles indicated here correspond to the $1/\sqrt{e}$ angular beam radius. The $1/e^2$ full angle beam divergence is equal to four times the angles indicated above.

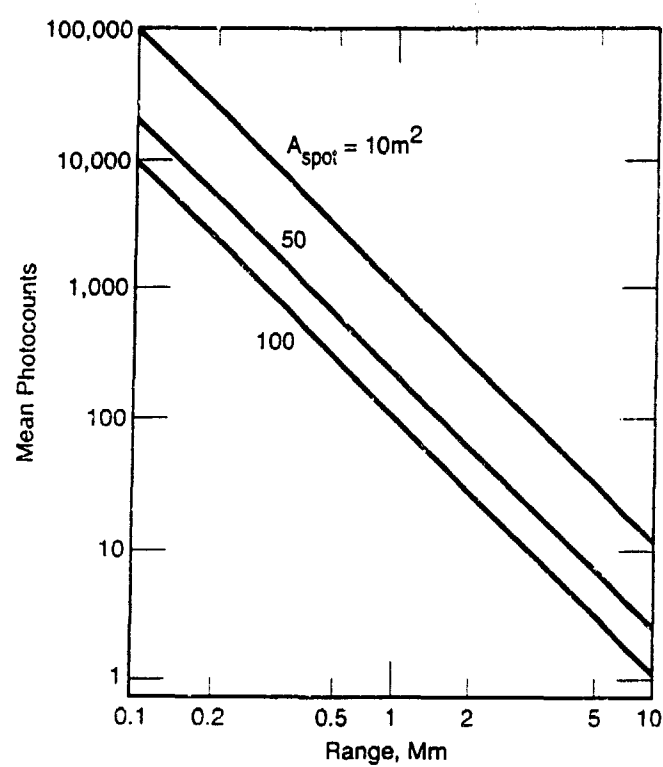


Figure 3. The mean number of signal photocounts as a function of range for various values of the laser spot area at the target.

In the second section, we develop elementary analytic expressions, suitable for commercially available spreadsheet programs, such as JAVELIN, for the probability of detection including the effects of both unintentional beam boresight error and beam jitter in the low photocount regime. In the third section, we consider the high photocount regime and develop analytical expressions for the corresponding probability of detection. Finally, in the Summary, we summarize the approximations of the detection probabilities obtained here, together with their respective regions of validity. Those readers who want to use directly the respective approximations, but do not want to get involved with the technical details, can skip to the final results in the Summary.

In order for this report to be as self-contained as possible, we have included a number of appendices to serve as technical references and document some interesting results that may not be well known. In Appendix A, we assume a LADAR system with circularly symmetric Gaussian jitter with a fixed pointing offset and derive the corresponding probability distribution of intensity. In Appendix B, we show how the general photoelectron count distribution, given by the negative-binomial probability distribution, reduces to the Gaussian (i.e., normal) distribution for both large photocounts and speckle numbers contained within the collecting aperture. In addition, we show how the negative-binomial distribution reduces to the Bose-Einstein and Poisson distribution in the limit that the speckle number tends to one and infinity, respectively. In Appendix C, we consider signal-noise-limited detection for large photoelectron counts and mean number of speckles near unity and derive the corresponding count distribution and probability of detection. In this regard, we have derived a possible new and interesting mathematical result involving the incomplete gamma function. Finally, in Appendix D, we consider the case of a signal obeying Bose-Einstein photocount statistics (such as that arising from unresolved targets), which is immersed in Poisson noise, and derive the photocount probability of signal plus noise as well as the corresponding probability of detection. In particular, we obtain a

closed-form, analytical expression for the probability distribution, valid for all values of signal and noise photocounts.

Probability of Detection for Low Photoelectron Counts

Detection Statistics without Pointing Errors

First consider the situation where the mean photocount number K_s is small, say less than about 50. For the example considered in the previous section, we have seen that the low photocount regime is expected to be obtained for ranges ≥ 1 Mm. For a LADAR system to be viable in this regime, it is necessary to assume that over a pulse-length, the background, and/or photodetector, noise is much smaller than the corresponding return signal strength. That is, in the low photocount regime, we assume a (near) quantum-noise-limited LADAR system. Such physical circumstances may be obtained for a space-based LADAR system with sufficiently narrow field-of-view and optical bandpass that operates in the natural environment against a deep space background (i.e., no earth, moon, sun, or stars in the field-of-view) and with the line-of-sight between the LADAR and the target having tangent altitudes greater than ~ 100 km. In addition, it is necessary to employ a sufficiently low-noise photodetector (e.g., a cooled photomultiplier or a semiconductor avalanche photodiode operating above breakdown in the triggered avalanche Geiger mode).

Since in the low photocount regime we assume negligible background and/or detector-induced noise photocounts over the measurement time of interest, the probability of a detection, P_d , of a single return signal pulse is equal to the probability that at least one photocount occurs during this time interval. This quantity is just equal to one minus the probability of obtaining zero counts during this time interval. Hence, from Eq. (6) we obtain

$$\begin{aligned}
 P_d &= 1 - P(0) \\
 &= 1 - \left(1 + \frac{K_s}{m}\right)^{-m}, \quad (9)
 \end{aligned}$$

where K_s is the mean number of signal photoelectron counts expected from the LADAR pulse, and m is the mean number of speckles of the diffuse reflected pulse contained within the collecting aperture.

In LADAR systems, where the probability of detection per pulse, P_d , is low, target detection algorithms, constructed from multiple pulse statistics, can be employed to increase the detection probability. For example, when N independent pulse measurements are combined, the probability of detecting at least one photocount from a burst of N pulses is obtained as

$$\begin{aligned}
 P_d(N) &= 1 - (1 - P_d)^N = 1 - P(0)^N \\
 &= 1 - \left(1 + \frac{K_s}{m}\right)^{-Nm} \quad (10)
 \end{aligned}$$

Thus, by combining N independent pulses, the mean photocount K_s per pulse needed for a specific detection probability is lowered, and, consequently, for a given K_s , the acquisition range is correspondingly extended. Of course, this improvement is at the cost of the energy to produce the added pulses and the time required to make the measurements.

Detection Statistics with Pointing Errors

In general, the effects of pointing errors result in a reduction of target illumination and a corresponding decrease in return-signal energy. As a result, the LADAR detection probability is reduced in comparison to the corresponding value in the absence of pointing errors. In the following, a fixed angular pointing offset bias and circularly symmetric Gaussian jitter are assumed.

The quantity P_d , given by Eq. (9), represents the detection probability of a single pulse without any pointing errors. The corresponding probability with beam jitter and offset is obtained by integrating P_d over the mean photocount distribution as a function of the pointing statistics. That is, with jitter and offset, the mean photocount is now considered as a random variable, k , with pointing statistics given by (see Appendix A)

$$P_{pt}(k) = \left[\frac{a^2 \exp(-a^2 b^2 / 2)}{K_s} \right] (k/K_s)^{a^2 - 1} J_0 \left(a^2 b \sqrt{2/n(k/K_s)} \right), \quad 0 \leq k \leq K_s,$$

$$= 0, \text{ otherwise } , \quad (11a)$$

where circularly symmetric Gaussian jitter statistics are assumed, J_0 is the Bessel function of the first kind of order zero, θ_{pt} is the (angular) pointing offset, σ_j is the single-axis Gaussian jitter standard deviation, and θ_0 is the Gaussian laser beam shape standard deviation.

$$a = \frac{\theta_0}{\sigma_j} \quad (11b)$$

$$b = \frac{\theta_{pt}}{\theta_0} \quad (11c)$$

θ_{pt} is the (angular) pointing offset, σ_j is the single-axis Gaussian jitter standard deviation, and θ_0 is the Gaussian laser beam shape standard deviation.

The probability of detection of a pulse with pointing errors, denoted by \bar{P}_d , is thus

$$P_d = \int_0^{K_s} P_d(k) P_{pt}(k) dk \quad (12)$$

where $P_d(k)$ is given by Eq. (9), with K_s replaced by k , and $P_{pt}(k)$ is given by Eq. (11).

In general, closed-form solution exists for this integral, although numerical results can be readily obtained on a digital computer.

One would not expect to design and employ a LADAR system with excessive pointing offset and jitter. To this end, we have derived an elementary engineering approximation for \bar{P}_d valid for $\sigma_j/\theta_0 \leq 0.5 - 0.75$ (or $a = \theta_0/\sigma_j \geq 1.5 - 2$), and $\theta_{pt}/\theta_0 \leq 1.0$. The most accurate approximation obtained so far that is suitable for spreadsheet programs is given by

$$\begin{aligned} \bar{P}_d &\approx P_d(\bar{K}_s) \\ &= 1 - \left(1 + \frac{\bar{K}_s}{m} \right)^{-m} \end{aligned} \quad (13)$$

where

$$\begin{aligned}\bar{K}_s &= \int_0^{\infty} k P_{pt}(k) dk \\ &\approx K_s \left(\frac{a^2}{a^2 + 1} \right) \exp \left[- \frac{b^2}{2} \left(\frac{a^2}{a^2 + 1} \right) \right]\end{aligned}\quad (14)$$

In obtaining the engineering expression given by Eq. (14), we expanded the Bessel function in Eq. (11) to terms of second order in b , performed the integration over k , and then exponentialized the result so that the limit of \bar{K}_s as $\sigma_j \rightarrow 0$ is identical to the exact answer; $\bar{K}_s = K_s \exp[-b^2/2]$.

A comparison of the exact numerical and approximate results are shown in Figures 4 through 9 for a wide range of the parameter values. We note that any practical LADAR system design would not allow the laser beam width, θ_0 , to be less than both the jitter standard deviation σ_j and the offset bias θ_{pt} . A reasonable design goal would limit both the ratio σ_j/θ_0 and θ_{pt} to be less than about 1/2 (i.e., $a \geq 2$, and $b \leq 0.5$). Examination of Figures 4 through 9 reveals that over a wide range of the parameters m and K_s , the approximate analytical result of Eq. (13) agrees within 10 percent of the numerical result for both $a \geq 2$ and $b \leq 1$. That is, in the range where a LADAR system should be designed, Eq. (13) represents a good engineering approximation for the probability of detection in the presence of jitter in the low photocount regime.

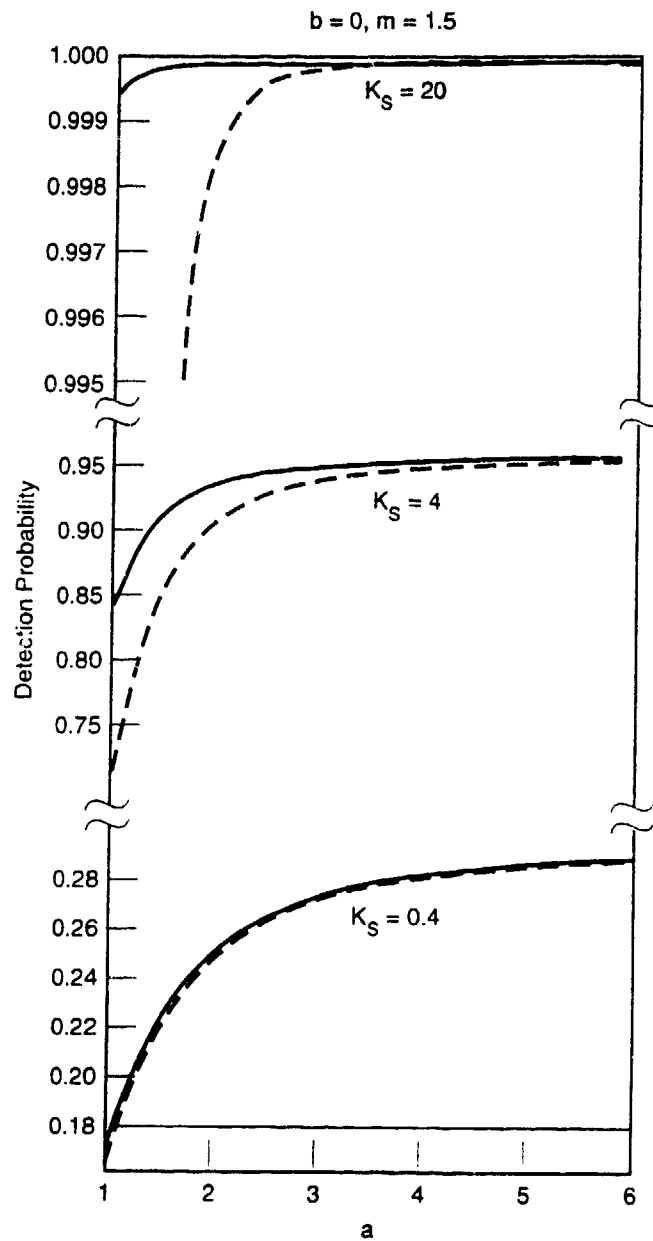


Figure 4. Probability of detection for the case where $m = 1.5$ and $b = 0$. The dashed curves are the exact numerical results, and solid curves are the approximate numerical results (given by Eq. 13), respectively.

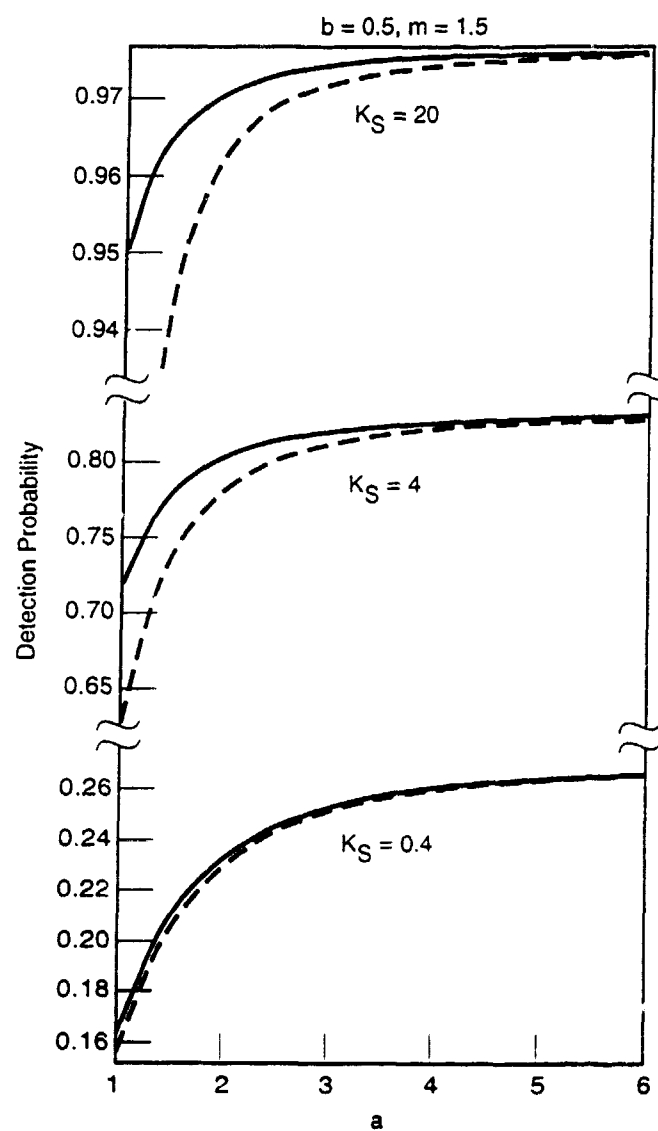


Figure 5. Probability of detection for the case where $m = 1.5$ and $b = 0.5$. The dashed curve is the numerical result, and solid curves are the numerical and approximate result (given by Eq. 13), respectively.

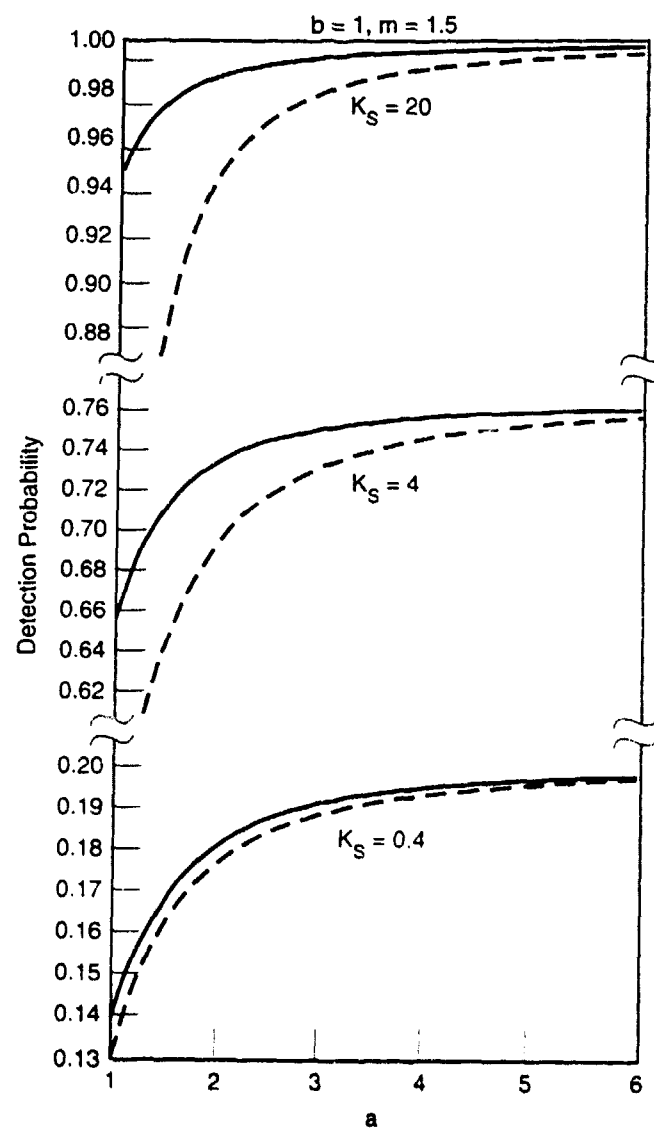


Figure 6. Probability of detection for the case where $m = 1.5$ and $b = 1$. The dashed curve is the numerical result, and solid curves are the numerical and approximate result (given by Eq. 13), respectively.

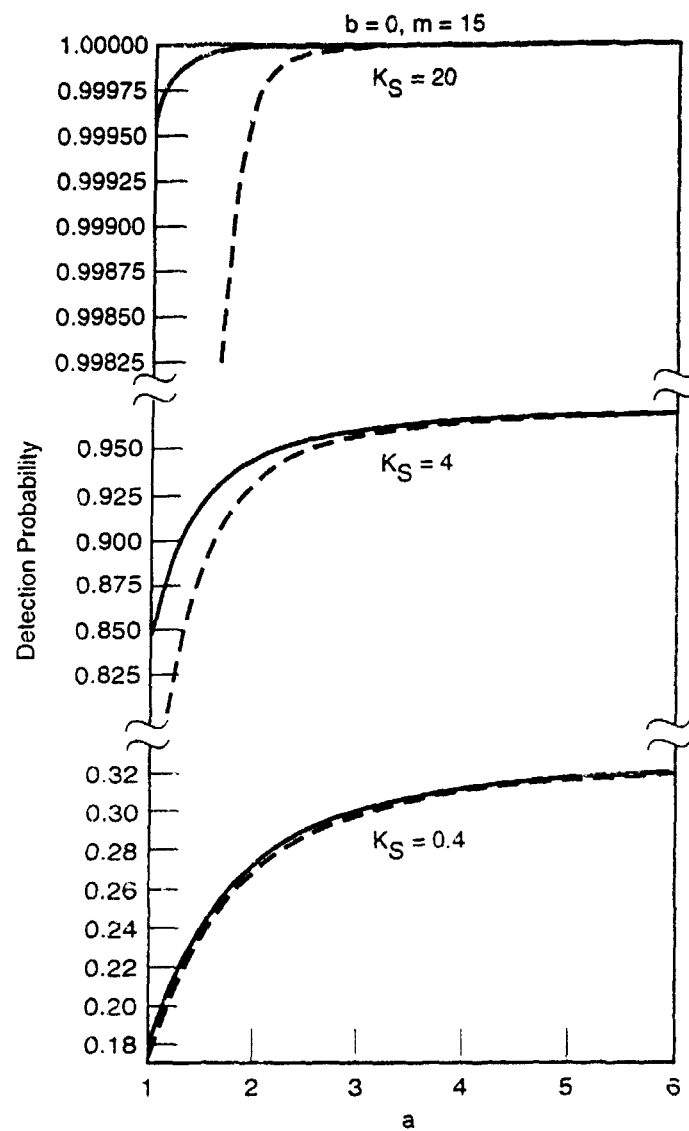


Figure 7. Probability of detection for the case where $m = 15$ and $b = 0$. The dashed curve is the numerical result, and solid curves are the numerical and approximate result (given by Eq. 13), respectively.

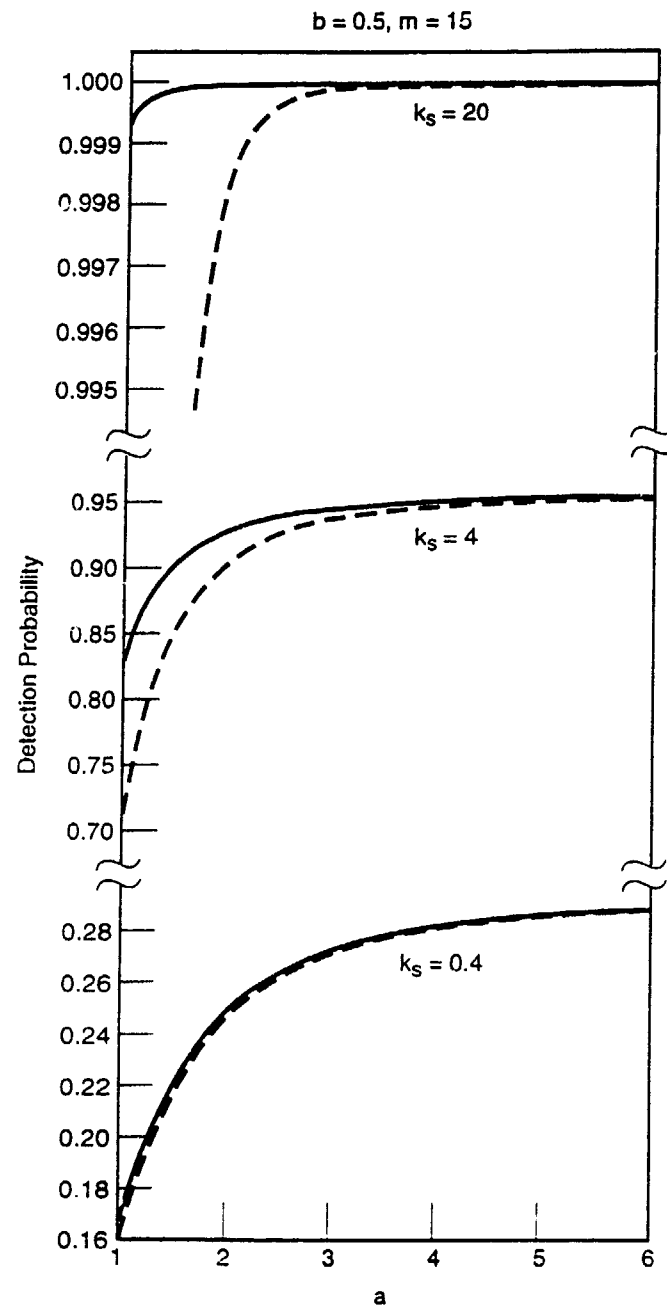


Figure 8. Probability of detection for the case where $m = 15$ and $b = 0.5$. The dashed curve is the numerical result, and solid curves are the numerical and approximate result (given by Eq. 13), respectively.

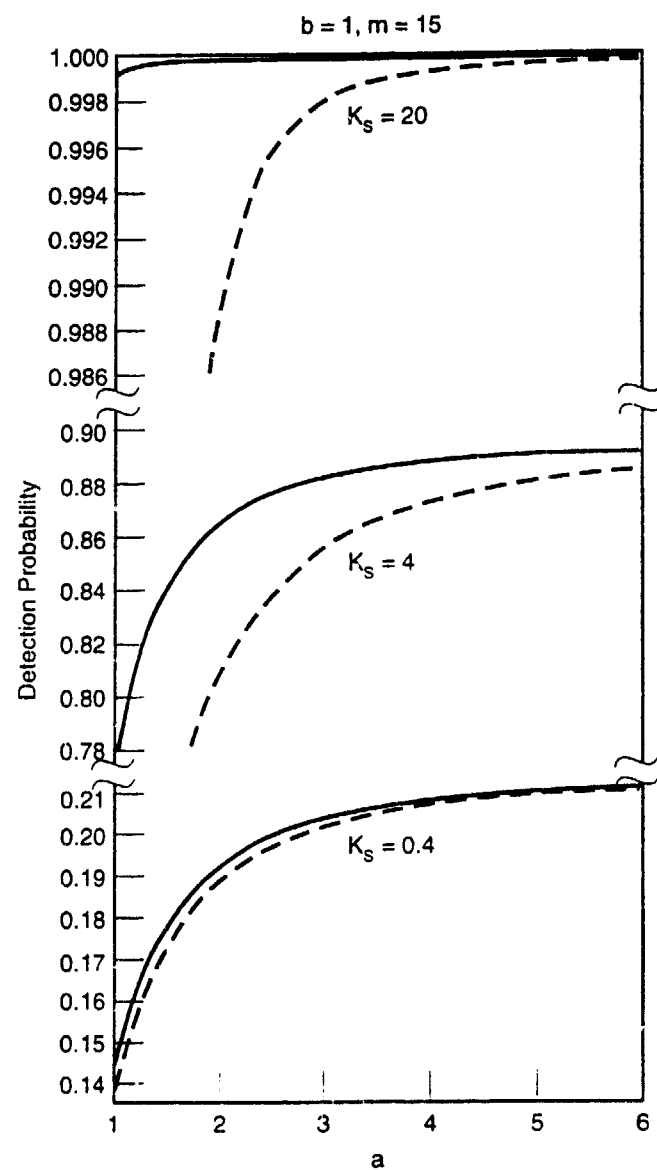


Figure 9. Probability of detection for the case where $m = 15$ and $b = 1$. The dashed curve is the numerical result, and solid curves are the numerical and approximate result (given by Eq. 13), respectively.

Probability of Detection for High Photoelectron Counts

Detection Statistics without Pointing Errors

Consider situations where a large number of both signal and noise photocounts per pulse are expected, such as a space-based LADAR system that views below the horizon. Following Goodman⁴ and Kingston¹ we assume that the total non-signal-related noise (i.e., background, dark current, thermal, etc) is Poisson distributed. For large photocounts, this distribution is to a very good approximation Gaussian. As discussed previously, it is customary in the high photocount regime to deal with currents rather than count number [see Eq. (8)]. Thus the ac component of the non-signal-related noise current from the detection system can be expressed as

$$P_n(i) = \frac{1}{\sqrt{2\pi\sigma_n^2}} \exp\left[-\frac{i^2}{2\sigma_n^2}\right], \quad (15)$$

where the non-signal noise current variance is given by

$$\sigma_n^2 = \frac{q^2}{T^2} K_B + \sigma_{dk}^2 + \sigma_{th}^2, \quad (16)$$

where K_B is the mean background photoelectron count per measurement interval T ($T \geq \tau$). σ_{dk}^2 and σ_{th}^2 are the dark current and thermal noise current variance, respectively.

The probability of false-alarm, P_{fa} , is obtained by integrating Eq. (15) above a measurement threshold current i_T . We thus obtain

$$P_{fa} = \frac{1}{2} \left[1 - \operatorname{erf} \left(\frac{(\operatorname{TNR})_o}{\sqrt{2}} \right) \right] , \quad (17)$$

where erf denotes the error function, and the threshold to (non-signal related) noise ratio is given by

$$(\operatorname{TNR})_o = \frac{i_T}{\sigma_n} \quad (18)$$

A curve fit to the numerical inversion of Eq. (17), which is accurate to better than 1 percent over the range $10^{-5} \leq P_{fa} \leq 10^{-2}$, is given by

$$(\operatorname{TNR})_o = 0.513 - 1.02 \log P_{fa} - 0.0539(\log P_{fa})^2 . \quad (19)$$

For example, a required false-alarm probability of 10^{-3} requires that the $(\operatorname{TNR})_o \approx 3.1$.

We note that P_{fa} is determined by the non-signal-related noise.

The probability distribution of signal photocounts is given by the negative-binomial distribution of Eq. (6). Now for both $K_s \gg 1$ and $m \gg 1$, it can be shown that probability distribution of the signal current distribution is also Gaussian and given by (see Appendix B)

$$P_s(i) \equiv \frac{1}{\sqrt{2\pi\sigma_s^2}} \exp \left[-\frac{(i - i_s)^2}{2\sigma_s^2} \right] , \quad (20)$$

where the mean signal current

$$i_s = \frac{qK_s}{\tau} , \quad (21a)$$

and

$$\sigma_s^2 = \frac{qi_s}{\tau} + \frac{i_s^2}{m} . \quad (21b)$$

The Gaussian probability distribution is a good approximation to the photoelectron distribution as long as the standard deviation is small compared to the mean. In practice, this is well satisfied for $K_s \geq 50-100$ and $m \geq 5-10$.

Since both the signal and noise are Gaussian variates, the probability distribution of both signal plus noise is also Gaussian and given by

$$P_{sn}(i) = \frac{1}{\sqrt{2\pi\sigma_{sn}^2}} \exp\left[-\frac{(i - i_s)^2}{2\sigma_{sn}^2}\right] , \quad (22)$$

where

$$\sigma_{sn}^2 = \sigma_s^2 + \sigma_n^2 . \quad (23)$$

The probability of detection is obtained by integrating P_{sn} above a measurement threshold current i_T . The result is given by

$$P_d = \frac{1}{2} \left[1 + \operatorname{erf} \left(\frac{i_s - i_T}{\sqrt{2} \sigma_{sn}} \right) \right] \quad (24)$$

We note that the probability of detection is a function of both the signal-to-noise ratio (SNR) and the threshold-to-noise ratio (TNR), where the noise includes the contribution due to signal fluctuations, as is evident in Eq. (23).

Next we consider the case of $K_s \gg 1$, but m near unity (≤ 10). In this case, it is more useful to return to the discrete counting distribution. Goodman³ has shown that the probability distribution of the total number (signal plus noise) of photoelectrons ejected during reception of a return pulse is given by

$$P_{sn}(K) = \left(\frac{m}{m + K_s} \right)^m \frac{\exp[-n]}{\Gamma(m)} \sum_{j=0}^K \frac{\Gamma(K - j + m)}{\Gamma(j + 1) \Gamma(K - j + 1)} n^j \left(\frac{K_s}{m + K_s} \right)^{K-j}, \quad (25)$$

where n is the mean number of non-signal-related noise photoelectrons emitted during the measurement period T (i.e., $n = T^2 \sigma_n^2 / q^2$). In general, it can be shown by methods discussed in Chapter 9 of Reference 3 that $E[K] = n + K_s$ and $\operatorname{Var}[K] = n + K_s + K_s^2/m$.

Although suitable for numerical computations on a digital computer, Eq. (25) is not useful for spreadsheet programs such as JAVELIN. Under certain circumstances, simplification of Eq. (25) can be obtained. For $K_s \gg 1$ and $K_s \gg n$ (i.e., signal-noise-limited detection), it can be shown that (see Appendix C)

$$P_m(K) = \frac{1}{\Gamma(m)} \left(\frac{m}{K_s} \right)^m \exp[-m K/K_s] K^{m-1} , \quad (26)$$

which is valid for $m \geq 1$. This is known as the gamma distribution. Converting to current and integrating Eq. (26) above a measurement threshold yields the probability of detection

$$P_d = \frac{\Gamma(m, \varepsilon_m)}{\Gamma(m)} , \quad (27)$$

where

$$\varepsilon_m = m \frac{i_T}{i_s} , \quad (28)$$

and $\Gamma(a, z)$ is the complementary incomplete gamma function given by⁵

$$\Gamma(a, z) = \int_z^{\infty} e^{-t} t^{a-1} dt \quad (29)$$

Although no analytical approximation exists for arbitrary m , closed-form expressions can be obtained for integer m . As a result, we present analytical results for P_d for the first few values of integer m .

$m = 1$;

$$P_d = \exp[-i_T/i_s] , \quad (30a)$$

$$m = 2;$$

$$P_d = e^{-\varepsilon_2}(\varepsilon_2 + 1) \quad , \quad (30b)$$

$$m = 3;$$

$$P_d = \frac{e^{-\varepsilon_3}}{2}(\varepsilon_3^2 + 2\varepsilon_3 + 2) \quad , \quad (30c)$$

$$m = 4;$$

$$P_d = \frac{e^{-\varepsilon_4}}{6}(\varepsilon_4^3 + 3\varepsilon_4^2 + 6\varepsilon_4 + 6) \quad , \quad (30d)$$

$$m = 5;$$

$$P_d = \frac{e^{-\varepsilon_5}}{24}(\varepsilon_5^4 + 4\varepsilon_5^3 + 12\varepsilon_5^2 + 24\varepsilon_5 + 24) \quad , \quad (30e)$$

$$m = 6;$$

$$P_d = \frac{e^{-\varepsilon_6}}{120}(\varepsilon_6^5 + 5\varepsilon_6^4 + 20\varepsilon_6^3 + 60\varepsilon_6^2 + 120\varepsilon_6 + 120) \quad , \quad (30f)$$

For noninteger m , it is suggested to smoothly interpolate Eqs. (30, a through f) between successive integers. For larger values of m , the expressions based on the Gaussian probability distribution of Eq. (22) with $\sigma_{sn} = \sigma_s$ should apply (see Appendix C). Hence for $m \geq 5-10$, we can employ P_d as given by Eq. (24).

Except for the case $m = 1$, we have not been able to obtain closed-form expressions for P_{sn} for $K_s \gg 1$, small m and finite n . For $m = 1$, it can be shown that (see Appendix D)

$$\begin{aligned}
P_{sn}(K) &= \frac{\exp[-(K-n)/K_s]}{K_s} \frac{\Gamma(K+1, n)}{\Gamma(K+1)} \\
&\approx \frac{\exp[-(K-n)/K_s]}{K_s} U(K-n) \quad , \quad (31)
\end{aligned}$$

where U is the unit step function. The probability distribution of signal plus noise current can thus be expressed as

$$P_{sn}(i) = \frac{\exp[-(i-i_n)/i_s]}{i_s} U(i-i_n) \quad , \quad (32)$$

where $i_n(=qn/T)$ is the mean non-signal-related noise current. The corresponding probability of detection is now obtained as

$$P_d \approx e^{-I_T/I_n} \quad , \quad (33)$$

where the threshold current is now measured relative to the noise floor current i_n .

Detection Statistics with Pointing Errors

Just as in the low photoelectron current regime, the most accurate approximation to include the effects of a pointing offset bias and jitter is to replace the mean signal (i_s or K_s) by the corresponding value obtained by averaging over the pointing error probability distribution

given by Eq. (11). That is, K_s (and i_s , since it is proportional to the signal photoelectron count) is replaced by \bar{K}_s (and the corresponding expression for \bar{i}_s) given by Eq. (14).

We consider the regime where both K and $m \gg 1$. In this case \bar{P}_d , the detection probability averaged over the pointing statistics, is obtained from Eq. (24) with i_s replaced by \bar{i}_s , where

$$\frac{\bar{i}_s}{i} = \left(\frac{a^2}{a^2 + 1} \right) \exp \left[-\frac{b^2}{2} \left(\frac{a^2}{a^2 + 1} \right)^2 \right] \quad (34)$$

Figures 10 through 12 show a comparison of the numerical and approximate results for the detection probabilities as a function of $a = \theta_0/\sigma_j$ for a representative range of parameter values. In these figures, the (current) SNR and the corresponding TNR are defined as

$$\text{SNR} = \frac{i_s}{\sigma_{sn}} \quad (35a)$$

and

$$\text{TNR} = \frac{i_t}{\sigma_{sn}} \quad (35b)$$

Note, in particular, that the noise variance, σ_{sn} , includes signal fluctuations, in contrast to the false-alarm probability, which is based on non-signal-related noise only.

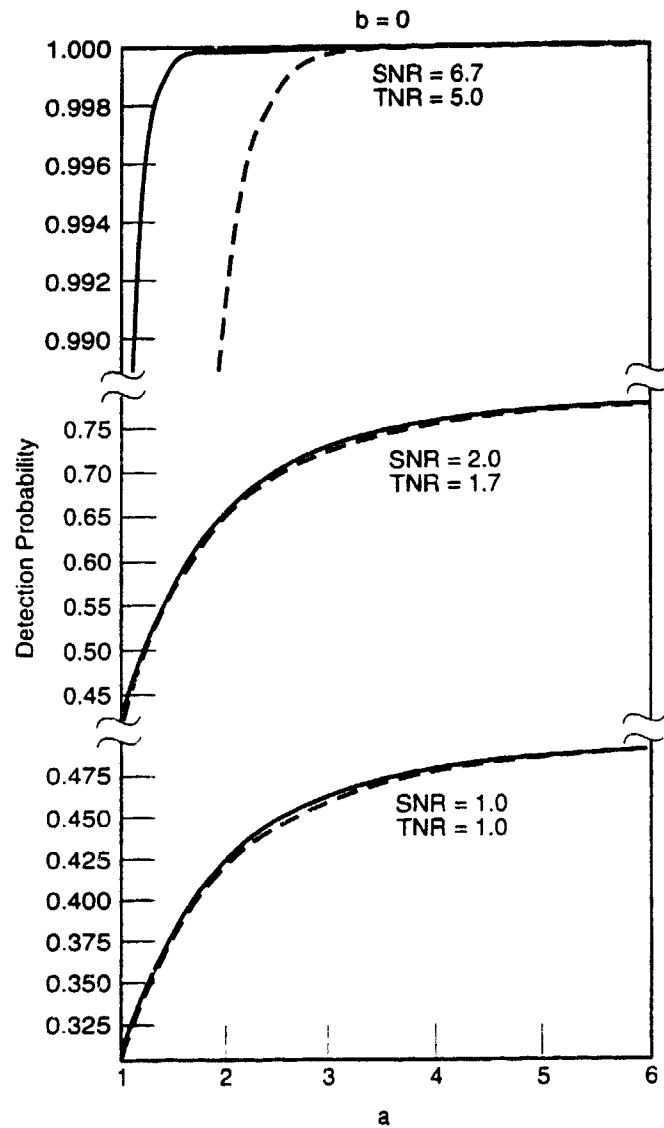


Figure 10. Probability of detection for a large number of photocounts and m is large ($\geq 5-10$) and $b = 0$. The dashed and solid curves are the numerical and approximate result, respectively.

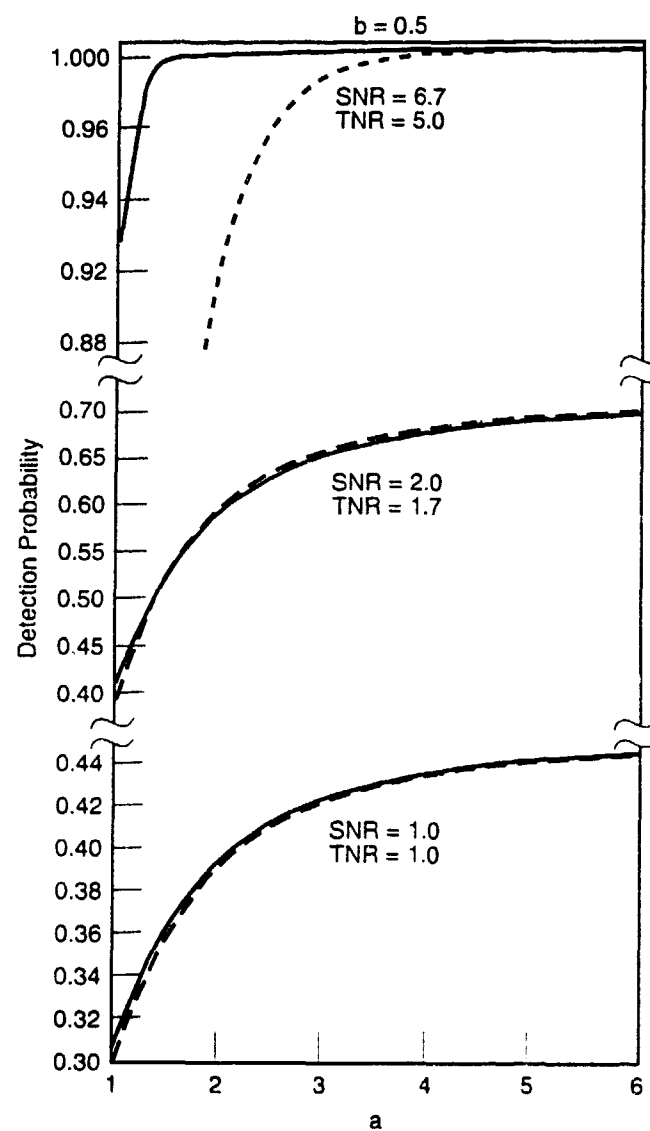


Figure 11. Probability of detection for a large number of photocounts and m is large ($\geq 5-10$) and $b = 0.5$. The dashed and solid curves are the numerical and approximate result, respectively.

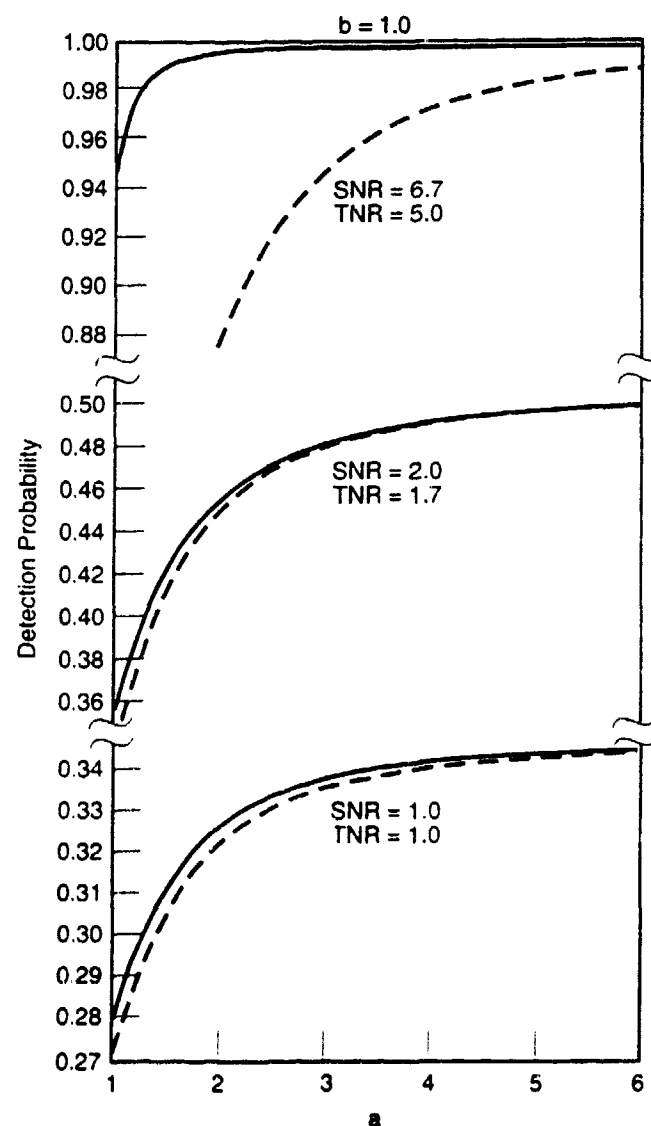


Figure 12. Probability of detection for a large number of photocounts and m is large ($\geq 5-10$) and $b = 1$. The dashed and solid curves are the numerical and approximate result, respectively.

Examination of Figures 10 through 12 reveals, as in the low photoelectron count regime, that the algorithm used here to include the effects of pointing errors is sufficient for use as an engineering approximation over the design range of a practical LADAR system. We note that evaluation of the error function may not be compatible with some spreadsheet programs. If this is the case, use of a global rational approximation to the error function can be employed, such as⁶:

$$\text{erf}(x) = 1 - (a_1 t + a_2 t^2 + a_3 t^3) e^{-x^2} + \varepsilon(x) \quad ,$$

where

$$|\varepsilon(x)| \leq 2.5 \times 10^{-5} \quad ,$$

$$t = \frac{1}{1 + px} \quad ,$$

and

$$p = 0.47047, a_1 = 0.34802, a_2 = -0.09587, \text{ and } a_3 = 0.74786 \quad .$$

Additionally, we consider the case of signal-limited-noise detection where $K_s \gg 1$, and m is near unity. In this case, we have from Eqs. (27) and (28)

$$\bar{P}_d = \frac{\Gamma(m, \bar{\varepsilon}_m)}{\Gamma(m)} \quad , \quad (36)$$

where

$$\bar{\epsilon}_m = m \frac{\bar{i}_T}{\bar{i}_s} = m \frac{\bar{i}_T}{\bar{i}_s} (i_s / \bar{i}_s) \quad , \quad (37)$$

and the ratio \bar{i}_s / i_s is given by Eq. (34). For low integer values of m , the results given by Eq. (30) are to be used with ϵ_m replaced by $\bar{\epsilon}_m$.

Figures 13 through 15 show a comparison of the numerical and approximate results for the detection probability as a function of θ_0 / σ_j for $m = 1$ and a representative range of parameters. The results for m greater than unity behave similarly. Examination of these figures reveals that the approximations obtained above are sufficient for engineering purposes.

Finally, we note, that when N multiple independent measurements are combined, the probability of detection becomes

$$P_d(N) = 1 - (1 - P_d)^N \quad , \quad (38)$$

where P_d is the detection probability of a single pulse.

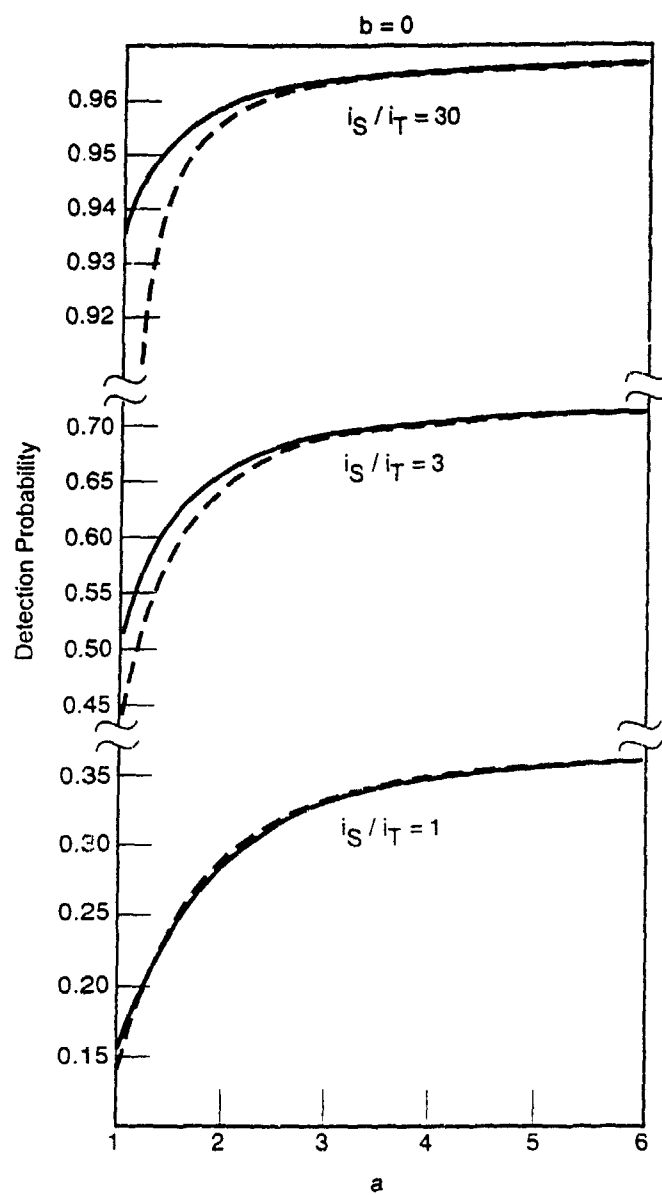


Figure 13. Probability of detection for $m = 1$, $b = 0$ and both the SNR and TNR are large. The dashed and solid curves are the numerical and approximate results, respectively.

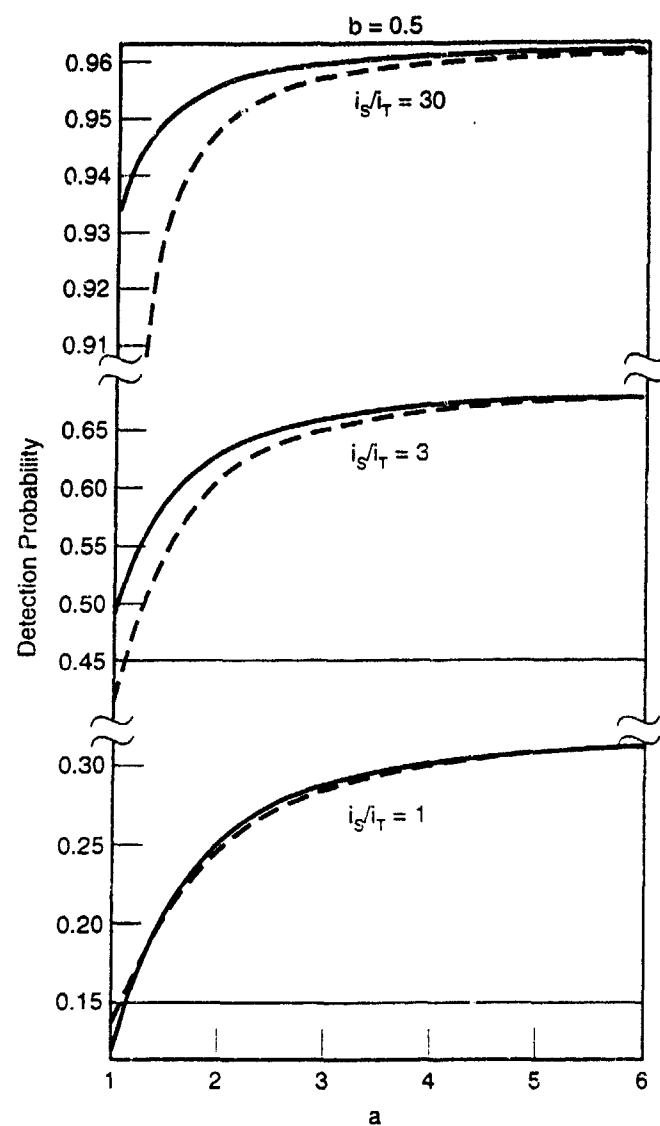


Figure 14. Probability of detection for $m \approx 1$, $b = 0.5$ and both the SNR and TNR are large. The dashed and solid curves are the numerical and approximate results, respectively.

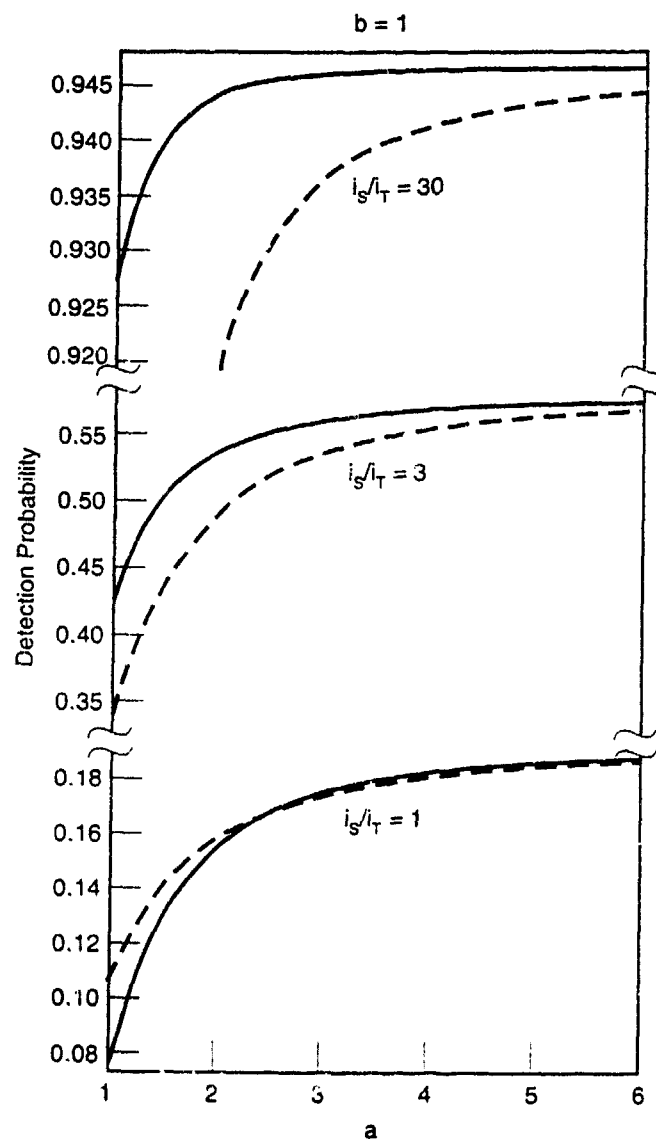


Figure 15. Probability of detection for $m \approx 1$, $b = 1$ and both the SNR and TNR are large. The dashed and solid curves are the numerical and approximate results, respectively.

Summary

In this report, we have derived accurate (to within 10 percent), elementary, analytical expressions for the probability of detection, \bar{P}_d , over a reasonable design goal range, of a monostatic, direct-detection LADAR system in the presence of unintentional pointing errors. We distinguish between two photocount regimes—low ($K_s \ll 100$) and high (K_s greater than 50–100). As discussed in the second section, in the low photocount regime, we are primarily interested in signal-noise-limited LADARs. In this regime, we obtain results for \bar{P}_d that are valid for resolved targets ($m > 10$), partially resolved targets ($1 < m < 5-10$), and unresolved targets ($m \approx 1$). On the other hand, in the high photocount regime, we obtain results for \bar{P}_d , valid for both $m \approx 1$ and $m \gg 1$ and arbitrary values of non-signal-related noise. For partially resolved targets, we have not been able to obtain elementary approximations of \bar{P}_d except for cases of large values of the $(\text{SNR})_o$,

where

$$(\text{SNR})_o = \frac{i_s}{\sigma_n} \quad (39)$$

is the signal-to-(non-signal-related) noise ratio.

In Table 1, we summarize several of the key parameters used here with a reference to their appearance in the body of the paper. For the low photocount regime ($K_s \ll 100$), the detection probability of a burst of N independent pulses, averaged over the pointing statistics, is given by

$$\bar{P}_d(N) = 1 - \left(1 + \frac{\alpha K_s}{m}\right)^{-mN}, \quad m \geq 1, \quad (40)$$

where

$$\alpha = \left(\frac{a^2}{a^2 + 1}\right) \exp\left[-\frac{1}{2}\left(\frac{ba^2}{a^2 + 1}\right)^2\right] \quad (41)$$

In Table 2, we summarize the results obtained for \bar{P}_d in the high photocount regime ($K_s \geq 50-100$). For a burst of N independent pulses the probability of detection is given by Eq. (38).

The approximations for \bar{P}_d given in Eq. (40) and Table 2 are accurate to within 10 percent for $a = \theta_0/\sigma_j > 2$, and $b = \theta_{pt}/\theta_0 < 1$. As such, these results should greatly aid parametric system modeling of (proposed) LADARs that are employed for both target ranging and analytical cost engineering modeling of corresponding space defense systems.

Table 1. Definitions of Some Key Parameters and Reference to Their Appearance in the Body of this Report. The quantities q , t , θ_{pt} , and σ_j are the charge on the electron, return-signal pulse-width, angular boresight error, and single-axis angular jitter standard deviation, respectively.

PARAMETER	VALUE	EQUATION NO./ COMMENTS
K_s	Mean signal photoelectron count per pulse	2
i_s	Mean signal current per pulse	qK_s/τ
m	Mean number of speckles contained within the collecting aperture	7
θ_0	Laser beam angular radius	4
σ_n^2	Non-signal related noise current variance	16
P_{fa}	Probability of false alarm	17
i_T	Threshold current	Obtained from Eq. (19)
a	θ_0/σ_j	11b
b	θ_{pt}/θ_0	11c
$\bar{\epsilon}_m$	$m \frac{i_T}{i_s}$	28
\bar{K}_d	Mean photoelectron count, averaged over the pointing statistics	14
\bar{P}_d	Detection probability per pulse, averaged over the pointing statistics	12

Table 2. Probability of Detection per Pulse, Averaged over the Pointing Statistics in the High Photoelectron Count Regime. The quantity α is given by Eq. (41).

m	\bar{P}_d	COMMENTS
≈ 1 (unresolved targets)	$\exp[-i_T/\alpha i_s]$	Valid for all values of noise.
$1 < m \leq 5-10$ (partially resolved targets)	$\frac{\Gamma(m, \epsilon_m/\alpha)}{\Gamma(m)}$	Valid for $(\text{SNR})_0 > 1$. For integer m, use Eq. (30) with ϵ_m replaced by ϵ_m/α . For noninteger values, smoothly interpolate between successive integers
$m > 10$ (resolved targets)	$\frac{1}{2} \left[1 + \operatorname{erf} \left(\frac{\alpha i_s - i_T}{\sqrt{2} \bar{\sigma}_m} \right) \right]$	Valid for all values of σ_{sn} . Use the rational approximation, given in Sec. IIIB, to the error function in spreadsheet programs. For a given σ_n and P_{fa} , the threshold current is obtained from Eqs. (18) and (19).

where

$$\bar{\sigma}_m = \sqrt{\frac{q\alpha i_s}{\tau} + \frac{(\alpha i_s)^2}{m} + \sigma_n^2}$$

References

1. R. H. Kingston, *Detection of Optical and Infrared Radiation*, (Springer Verlag Publishing Co., New York, 1979).
2. C. G. Bachman, *Laser Radar Systems and Techniques*, (Artech House Inc., Dedham, MA, 1979), Chap. 2.
3. J. W. Goodman, *Statistical Optics*, (John Wiley & Sons, New York, 1985), Chap.9.
4. J. W. Goodman, "Some Effects of Target-Induced Scintillation on Optical Radar Performance," *Proc. IEEE*, **53**, 1688-1700 (1965).
5. L. C. Andrews, *Special Functions for Engineers and Applied Mathematicians*, (Macmillan Pub. Co., New York, 1985), Chap. 2.
6. M. Abramowitz and I. A. Stegun, *Handbook of Mathematical Function*, (Dover Publishing, New York, 1965), Chap. 7.
7. P. Beckman, *Probability in Communication Engineering*, (Harcourt Brace & World Inc., New York, 1967), Chap.4.
8. A. P. Prudnikov, Yu, A. Brychov, and O. I. Marichev, *Integrals and Series, Vol. 1, Elementary Functions*, (Gordon Breach Science Publishers, New York, 1986) Chap. 4.

Appendix A

Pointing-error Statistics

In this Appendix, we outline the derivation of Eq. (11). We assume circularly symmetric Gaussian angular jitter statistics with a fixed angular offset bias for the LADAR's pointing system. Let θ denote the angle with respect to the direction of the target at which the beam points at any instant of time. The probability density of θ being in the range θ to $\theta + d\theta$ is given by the Rice-Nakagami distribution.⁶ In the notation used here this distribution is given by

$$P_{pt}(\theta) = \frac{\theta}{\sigma_j^2} \exp\left[-\frac{\theta^2 + \theta_{pt}^2}{2\sigma_j^2}\right] I_0\left(\frac{\theta\theta_{pt}}{\sigma_j^2}\right) , \quad (A-1)$$

where I_0 is the modified Bessel function of order zero, σ_j is the single-axis angular jitter standard deviation, and θ_{pt} is the corresponding offset bias. The corresponding probability density of irradiance on the target, $P_{pt}(I)$, can be obtained from $P_{pt}(\theta)$ through the relation

$$P_{pt}(I) = \left| \frac{d\theta}{dI} \right| P_{pt}(\theta) \quad (A-2)$$

For a given θ , the irradiance at the target location is given

$$I(\theta) = I_0 \exp\left[-\theta^2/2\theta_0^2\right] ,$$

from which it follows that

$$\theta = \sqrt{-2\theta_0^2 \ln[I/I_0]} \quad , \quad (\text{A-3})$$

Differentiating Eq. (A-3) with respect to I and substituting this result together with Eq. (A-1) into Eq. (A-2) yields, after algebraic simplification,

$$P_{pt}(I) = \left[\frac{a^2 e^{-a^2 b^2/2}}{I_0} \right] (I/I_0)^{a^2-1} J_0(a^2 b \sqrt{2 \ln(I/I_0)}) \quad , \quad 0 \leq I \leq I_0 \quad (\text{A-4})$$

$$= 0, \text{ otherwise } ,$$

where J_0 is the Bessel function of the first kind of order zero, $a = \theta_0/\sigma_j$, and $b = \theta_{pt}/\theta_0$. By noting that the signal photoelectron count (and corresponding signal current) is directly proportional to the target illumination, Eq. (11) follows directly from Eq. (A-4).

Although in general no closed form integral exists for Eq. (12), we can, however, obtain an analytic result for the special case of no boresight pointing error (i.e., $b = 0$). With P_d given by Eq. (9), it can be shown that the probability of detection per pulse, averaged over the jitter distribution, is given by

$$\bar{P}_d = 1 - {}_2F_1[a^2, m; 1 + a^2; -K_s/m] \quad , \quad (\text{A-5})$$

where ${}_2F_1(a, b, c; z)$ is the hypergeometric function (discussed in Chapter 15 of Reference 6). Numerical results, based on Eq. (A-5), are shown in Figure 4 and 7. In the limit $m \rightarrow \infty$ (i.e., Poisson statistics) Eq. (A-5) yields $\bar{P}_d = 1 - {}_1F_1(a^2, 1 + a^2; -K_s)$, where ${}_1F_1(a, b; z)$ is the confluent hypergeometric function (see Sec. 9.2 of Ref. 5).

Appendix B

The Negative-binomial Distribution: Some Limiting Cases

First consider the case of large K_s and m . Substituting Stirling's approximation (i.e., $\Gamma(z+1) \cong \sqrt{2\pi} z^{z+1/2} e^{-z}$) for the gamma functions appearing in Eq. (6), we obtain

$$P_s(K) = \frac{1}{\sqrt{2\pi}} e^{f(K)} \quad , \quad (B-1)$$

where

$$\begin{aligned} f(K) = & (K + m - \tfrac{1}{2}) \ell n(K + m) - (K + \tfrac{1}{2}) \ell n(K) - (m - \tfrac{1}{2}) \ell n(m) \\ & - K \ell n\left(\frac{K_s + m}{K_s}\right) - m \ell n\left(\frac{K_s + m}{m}\right) \quad . \end{aligned} \quad (B-2)$$

For large K_s , we expect that $P(K)$ is peaked near $K \sim K_s$. Indeed, differentiating $f(K)$ with respect to K yields $f'(K) = \ell n\left(\frac{1 + m/K}{1 + m/K_s}\right)$, where terms of the order $1/K$, $1/m$, and higher are neglected.

From the condition $f'(K) = 0$ we obtain that the maximum value of f is achieved at

$$K = K_s \quad (B-3)$$

Thus, expanding $f(K)$ in a Taylor's series about K_s yields to terms of second order

$$\begin{aligned} f(K) &\cong f(K_s) + (K - K_s)f'(K_s) + \frac{1}{2}(K - K_s)^2 f''(K_s) \\ &= -\frac{1}{2} \ell n \sigma_K^2 - \frac{(K - K_s)^2}{2\sigma_K^2} \end{aligned} \quad (B-4)$$

where

$$\sigma_K^2 = K_s + \frac{K_s^2}{m} \quad (B-5)$$

Hence, from Eq. (B-4) and Eq. (B-1), we obtain

$$P_s(K) = \frac{1}{\sqrt{2\pi\sigma_K^2}} \exp \left[-\frac{(K - K_s)^2}{2\sigma_K^2} \right] \quad (B-6)$$

Thus, for large K_s and m , the negative-binomial distribution is Gaussian, with the same mean and variance of the underlying distribution. The corresponding probability distribution of signal current, Eq. (20), follows directly from Eq. (B-6) since $i = qK/\tau$. In particular, we have $\sigma_i^2 \equiv \text{Var}[i] = (q/\tau)^2 \text{Var}[K] = (q/\tau)^2 (K_s + K_s^2/m) = qi_s/\tau + i_s^2/m$, where the mean signal current $i_s = qK_s/\tau$.

An elementary argument involving the Central Limit theorem can be employed to derive Eq. (B-6) directly. Each of the m independent correlation cells or speckles contained with the

collecting aperture leads to a photocount distribution that obeys Bose-Einstein statistics with a mean count $k_s = K_s/m$, and a variance $\sigma_k^2 = k_s + k_s^2 = K_s/m + (K_s/m)^2$. The total photocount from the entire collecting aperture is just the sum of the (non-zero) contributions from each of the m independent correlation cells. The photocount, k , due to a single correlation cell is of the order K/m . Hence for k to be non-zero, it follows that K must be large since $m \gg 1$. Thus, for both large m and K we have, by the Central Limit theorem, the resulting probability distribution approaches the Gaussian distribution with a mean equal to $mk_s = K_s$ and a variance equal to $m\sigma_k^2 = K_s + K_s^2/m$, in agreement with Eq. (B-6).

Next consider the negative-binomial distribution in the limit $m \rightarrow 1$. In this case, we obtain from Eq. (6)

$$P_s(K) = \frac{1}{1 + K_s} \left(\frac{K_s}{1 + K_s} \right)^K, \quad m = 1 \quad (B-7)$$

This is known as the Bose-Einstein (or geometric) distribution. For large photoelectron counts, we have $(K_s/K_s + 1)^K \approx \exp(-K/K_s)$, and, hence, Eq. (B-7) becomes

$$P_s(K) \approx \frac{\exp(-K/K_s)}{K_s}, \quad (B-8)$$

which is known as the Rayleigh (or negative-exponential) distribution.

On the other hand, consider the limit of the negative-binomial distribution as $m \rightarrow \infty$. From Eq. (6), we have

$$\begin{aligned}
P_s(K) &= \frac{1}{K!} \lim_{m \rightarrow \infty} \left\{ \frac{\Gamma(K+m)}{\Gamma(m)} \left[1 + \frac{m}{K_s} \right]^{-K} \left[1 + \frac{K_s}{m} \right]^{-m} \right\} \\
&= \frac{1}{K!} m^K \left(\frac{K_s}{m} \right)^K e^{-K_s} \\
&= \frac{K_s^K e^{-K_s}}{K!} ,
\end{aligned} \tag{B-9}$$

which is the Poisson distribution.

Finally, we show that for large K , the Poisson distribution becomes a Gaussian distribution with a mean equal to K_s and a variance equal to the mean. Of course, this result follows directly from Eq. (B-6). However, since the Poisson distribution is interesting in its own right and plays such an important role in probability and statistics, we give an independent derivation, that starts directly from the Poisson distribution itself. For large K , we may use Stirling's approximation for $K!$ and express the Poisson distribution as

$$P(K) = \frac{1}{\sqrt{2\pi}} e^{g(K)} , \tag{B-10}$$

where

$$g(K) = K + K \ln K_s - \left(K + \frac{1}{2} \right) \ln K - K_s . \tag{B-11}$$

This function has a stationary point, for large K , at $K \approx K_s$. Expanding $g(K)$ in a second order Taylor series about $K = K_s$ yields

$$g(K) \approx -\frac{1}{2} \ln K_s - \frac{(K - K_s)^2}{2K_s} \quad (\text{B-12})$$

Hence, substituting Eq. (B-12) into Eq. (B-10) yields

$$P(K) = \frac{1}{\sqrt{2\pi K_s}} \exp \left[-\frac{(K - K_s)^2}{2K_s} \right] , \quad (\text{B-13})$$

which is the Gaussian distribution with the variance equal to the mean.

Appendix C

Signal-noise-limited Detection Statistics

In this appendix, we consider signal-noise-limited detection statistics where the mean number of signal photoelectrons per pulse $K_s \gg 1$, and the mean number of non-signal-related noise photoelectrons is negligible. The negative-binomial distribution given by Eq. (6) is

$$P_s(K) = \frac{\Gamma(K+m+1)}{\Gamma(m)\Gamma(K)} \left(1 + \frac{m}{K_s}\right)^{-K} \left(1 + \frac{K_s}{m}\right)^{-m} \quad (C-1)$$

For $K_s \gg 1$, $P_s(K)$ is nonzero for K large. In this case, we have

$$\Gamma(K+m-1) \cong K^{m-1} \Gamma(K)$$

and

$$\left(1 + \frac{m}{K_s}\right)^{-K} \cong \exp\left[-\frac{mK}{K_s}\right]$$

Thus

$$P_s(K) \cong \frac{1}{\Gamma(m)} \left(\frac{m}{K_s}\right)^m K^{m-1} \exp\left[-\frac{mK}{K_s}\right] \quad (C-2)$$

Next we show that for large K_s and m the detection probability, P_d , given by Eq. (27) is identical to that obtained from Eq. (24) in limit $n \rightarrow 0$. From Eq. (27), we have

$$P_d = \frac{\Gamma(m, m\epsilon)}{\Gamma(m)}$$

$$= \frac{1}{\Gamma(m)} \int_{m\epsilon}^{\infty} e^{-t} t^{m-1} dt \quad . \quad (C-3)$$

For large m , the integrand in Eq. (C-3) is peaked about $t = m - 1$. We now approximate the integrand in a particular way, by writing it in an exponential form, $\exp [f(t)]$, and using a Taylor series approximation for $f(t)$ near its maximum. (A Taylor's expansion of the integrand itself, for example, would not be useful if only a few terms are kept.) The integrand of Eq. (C-3) is

$$e^{f(t)} = t^{m-1} e^{-t} = \exp[(m-1)\ln t - t] \quad ,$$

so

$$f(t) = (m-1)\ln t - t$$

$$f'(t) = \frac{m-1}{t} - 1, \quad f' = 0 \text{ for } t = m-1$$

$$f'' = -\frac{(m-1)}{t^2} \quad ;$$

then, expanding about $t = m - 1$ yields

$$\begin{aligned}
P_d &= \frac{(m-1)^{m-1} \exp[-(m-1)]}{\Gamma(m)} \int_{m\varepsilon}^{\infty} \exp\left[-\frac{\{t-(m-1)\}^2}{2(m-1)}\right] dt \\
&= \frac{\sqrt{\pi/2(m-1)} (m-1)^{m-1} \exp[-(m-1)]}{\Gamma(m)} \\
&\quad \times \left(1 + \operatorname{erf}\left[\frac{\sqrt{m-1}(1-\varepsilon)}{\sqrt{2}}\right]\right) .
\end{aligned} \tag{C-4}$$

For large m , $\Gamma(m) \approx \sqrt{2\pi}(m-1)^{(m-1/2)} \exp[-(m-1)]$. Substituting this into Eq. (C-4) yields

$$P_d = \frac{1}{2} \left(1 + \operatorname{erf}\left[\frac{\sqrt{m}(1-\varepsilon)}{\sqrt{2}}\right]\right) . \tag{C-5}$$

which is identical to Eq. (24) for $\sigma_{sn}^2 = \sigma_s^2 = K_s^2/m$. Thus, in the limit of large m , Eq. (24) and Eq. (27) are identical for signal-noise-limited detection. In Figure C-1, we have compared these two expressions for $m = 5$ and 10. For engineering purposes, use of Eq. (24) for $m \geq 5$ should be adequate. Incidentally, it follows directly from Eq. (C-3) and (C-5) that

$$\lim_{m \rightarrow \infty} \frac{\Gamma(m, m\varepsilon)}{\Gamma(m)} = \begin{cases} 1, & 0 \leq \varepsilon < 1 \\ 1/2, & \varepsilon = 1 \\ 0, & \varepsilon > 1 \end{cases} . \tag{C-6}$$

This interesting result, to the best of my knowledge, has not yet appeared explicitly in the literature.

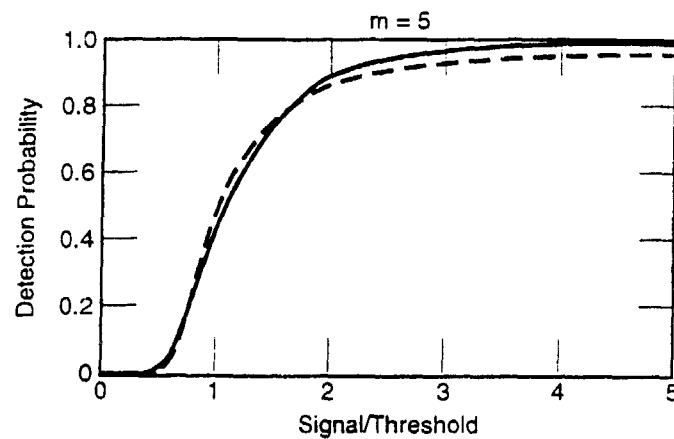
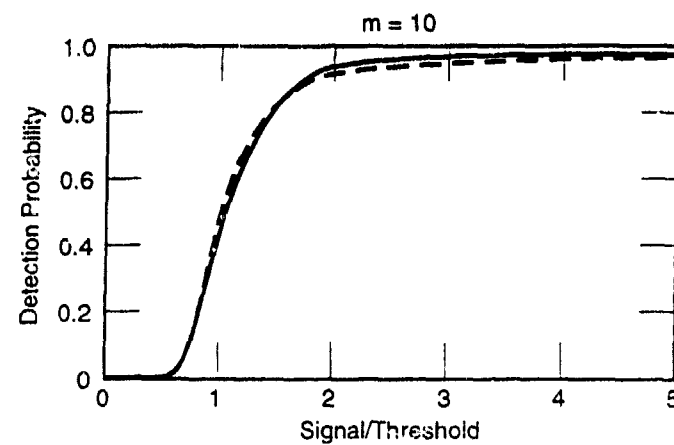


Figure C-1. Signal-noise-limited detection: a comparison of the detection probability as a function of the signal-to-threshold ratio. The dashed curve is based on Eq. (24) and the solid curve is based on Eq. (27).

Appendix D **Probability Distribution of a Signal Photoelectron Count Obeying Bose-Einstein Statistics Immersed in Poisson Noise**

For $m = 1$, Eq. (25) becomes

$$P_m = \left(\frac{1}{1 + K_s} \right) \left(1 + \frac{1}{K_s} \right)^{-K} e^{-n} \sum_{j=0}^K \frac{\beta^j}{j!} , \quad (D-1)$$

where

$$\beta = n(1 + K_s^{-1}) . \quad (D-2)$$

The sum appearing in Eq. (D-1) exists in closed form.⁸ The result is

$$\sum_{j=0}^K \frac{\beta^j}{j!} = e^{\beta} \frac{\Gamma(K+1, \beta)}{\Gamma(K+1)} , \quad (D-3)$$

where $\Gamma(a, z)$ is the complementary incomplete gamma function. Substituting Eq. (D-3) into Eq. (D-1) yields

$$P_m(K) = \frac{\left(1 + \frac{1}{K_s}\right)^{-K}}{1 + K_s} \exp[n/K_s] \frac{\Gamma(K+1, n + \frac{n}{K_s})}{K!} , \quad K = 0, 1, 2, \dots , \quad (D-4)$$

which is valid for arbitrary value of the mean photoelectron count, K_s , and non-signal-related mean photoelectron count, n . It can be shown for arbitrary K_s and n that $E[K] = K_s + n$ and $\text{Var}[K] = K_s + K_s^2 + n$.

In Figures D-1 through D-4, we plot P_{sn} as a function of K for a representative range of values of K_s and n . Except for large photocounts, no further simplification of Eq. (D-4) has been obtained. For $K_s \gg 1$, Eq. (D-4) can be written as

$$P_{sn}(K) \approx \frac{\exp [-(K-n)/K_s]}{K_s} G(K,n) , \quad (D-5)$$

where

$$G(K,n) = \frac{\Gamma(K+1,n)}{\Gamma(K+1)} . \quad (D-6)$$

Following the procedure outlines in Appendix B, it can be shown for large K that

$$G = \begin{cases} 0, & K < n \\ 1/2, & K = n \\ 1, & K > n \end{cases} . \quad (D-7)$$

That is, G behaves as a unit step-function located at $K = n$. These features are illustrated in Figure D-5 for $K \sim 1000$. Hence,

$$P_{sn} \approx \frac{\exp [-(K-n)/K_s]}{K_s} U(K-n) , \quad (D-8)$$

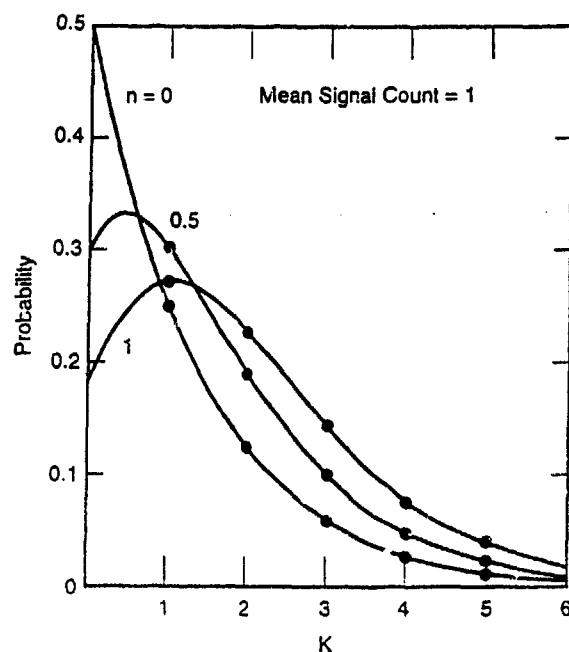


Figure D-1. Probability density of a signal obeying Bose-Einstein statistics immersed in Poisson noise, where the mean signal count = 1 for various values of the noise count. For convenience of presentation, a continuous curve is drawn between integer count values.

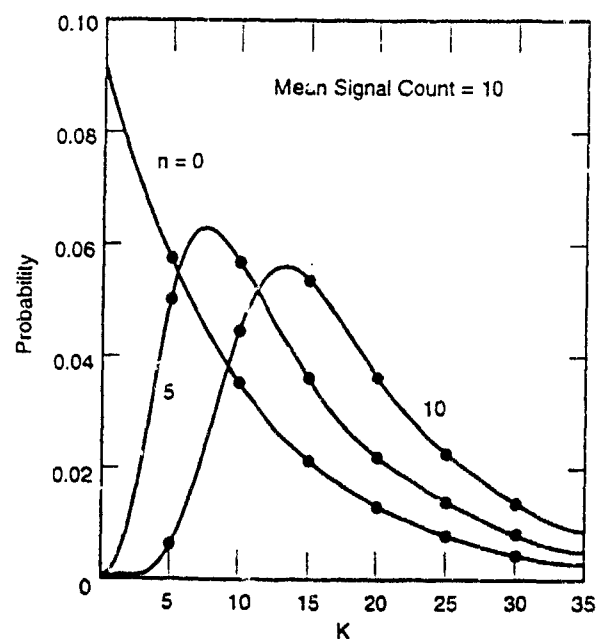


Figure D-2. Probability density of a signal obeying Bose-Einstein statistics immersed in Poisson noise, where the mean signal count = 10 for various values of the noise count.

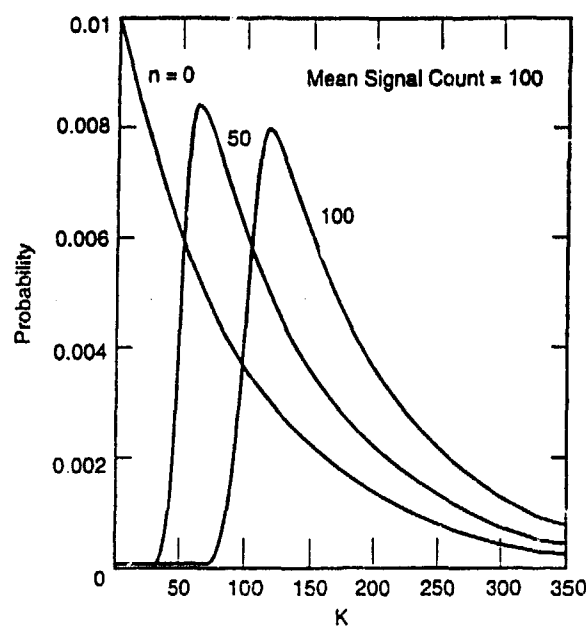


Figure D-3. Probability density of a signal obeying Bose-Einstein statistics immersed in Poisson noise, where the mean signal count = 100 for various values of the noise count.

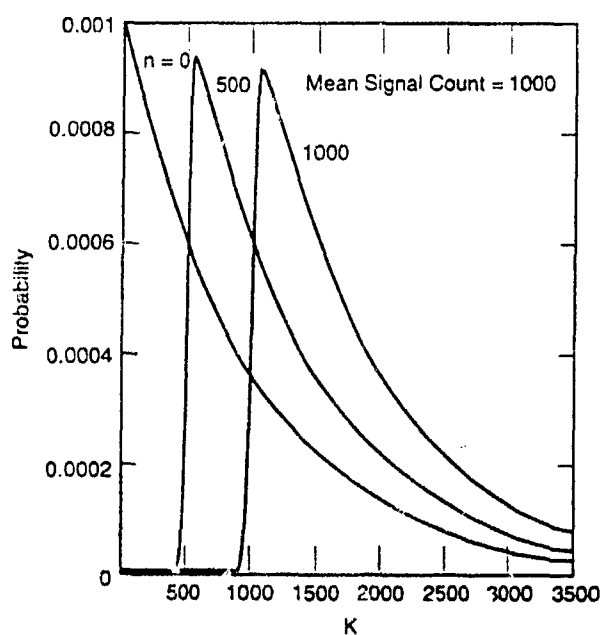


Figure D-4. Probability density of a signal obeying Bose-Einstein statistics immersed in Poisson noise, where the mean signal count = 1000 for various values of the noise count.

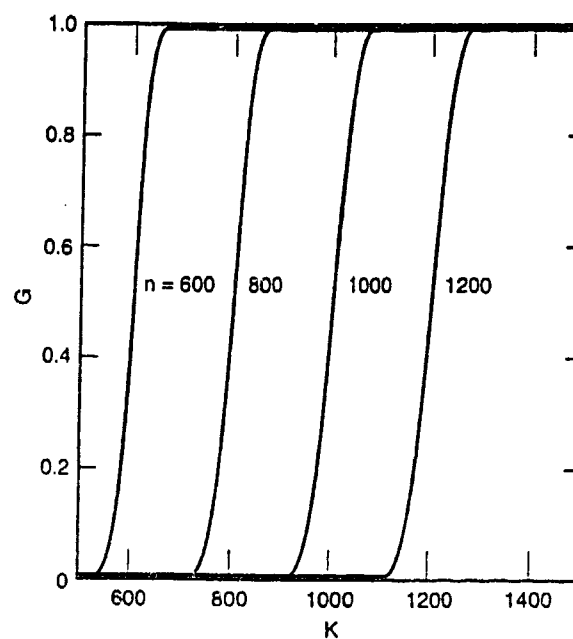


Figure D-5. Quantity $G(K, n) = \Gamma(K + 1, n)/\Gamma(K + 1)$ for photocounts near 1000 and various values of n .

where U is the unit step-function. Thus, in this limit, the probability of signal plus noise photoelectron counts is a shifted Bose-Einstein distribution, the shift being equal to the mean noise photocount. The corresponding probability of detection is given by

$$\begin{aligned}
 P_d &= \int_{K_T}^{\infty} P_m(K) dK \\
 &= \int_{n+\Delta K_T}^{\infty} P_m(K) dK \\
 &= e^{-\Delta K_T/K_s} \quad , \quad (D-9)
 \end{aligned}$$

where ΔK_T is the threshold count relative to the noise floor count, n . For large counts, where one operationally measures a current rather than discrete electron counts, the probability of detection is given by $\exp(-i_T/i_s)$, where i_T is the threshold current relative to the mean non-signal related noise current, i_n , and i_s is the corresponding mean signal current. Unfortunately, other than for $m = 1$, no analytic closed-form expressions have been obtained for Eq. (25).

Finally, consider the limit of the probability of emission of K signal plus noise photoelectrons, where the mean signal photocount is much less than the corresponding noise photocount (i.e., $K_s \ll n$). In this case we may use the asymptotic expansion of the complementary incomplete gamma function⁵,

$$\Gamma(a, z) \approx e^{-z} z^{a-1} \left(1 + \frac{a-1}{z} + \dots \right) \quad , \quad (D-10)$$

in Eq. (D-4) to obtain

$$\begin{aligned}
 P_{sn} &= \frac{(1+K_s^{-1})^{-K}}{1+K_s} e^{n/K_s} e^{-n-n/K_s} \frac{n^K (1+K_s^{-1})^K (1+KK_s/n)}{K!} \\
 &= \left(\frac{1}{1+K_s} \right) \frac{e^{-n} n^K (1+KK_s/n)}{K!} \\
 &= \frac{\exp[-(n+K_s)] (n+K_s)^K}{K!} ,
 \end{aligned} \tag{D-11}$$

to first order in K_s . Thus, for $K_s \ll n$ and arbitrary values of n , the statistics of the total emission process are Poisson.

TECHNOLOGY OPERATIONS

The Aerospace Corporation functions as an "architect-engineer" for national security programs, specializing in advanced military space systems. The Corporation's Technology Operations supports the effective and timely development and operation of national security systems through scientific research and the application of advanced technology. Vital to the success of the Corporation is the technical staff's wide-ranging expertise and its ability to stay abreast of new technological developments and program support issues associated with rapidly evolving space systems. Contributing capabilities are provided by these individual Technology Centers:

Electronics Technology Center: Microelectronics, solid-state device physics, VLSI reliability, compound semiconductors, radiation hardening, data storage technologies, infrared detector devices and testing; electro-optics, quantum electronics, solid-state lasers, optical propagation and communications; cw and pulsed chemical laser development, optical resonators, beam control, atmospheric propagation, and laser effects and countermeasures; atomic frequency standards, applied laser spectroscopy, laser chemistry, laser optoelectronics, phase conjugation and coherent imaging, solar cell physics, battery electrochemistry, battery testing and evaluation.

Mechanics and Materials Technology Center: Evaluation and characterization of new materials: metals, alloys, ceramics, polymers and their composites, and new forms of carbon; development and analysis of thin films and deposition techniques; nondestructive evaluation, component failure analysis and reliability; fracture mechanics and stress corrosion; development and evaluation of hardened components; analysis and evaluation of materials at cryogenic and elevated temperatures; launch vehicle and reentry fluid mechanics, heat transfer and flight dynamics; chemical and electric propulsion; spacecraft structural mechanics, spacecraft survivability and vulnerability assessment; contamination, thermal and structural control; high temperature thermomechanics, gas kinetics and radiation; lubrication and surface phenomena.

Space and Environment Technology Center: Magnetospheric, auroral and cosmic ray physics, wave-particle interactions, magnetospheric plasma waves; atmospheric and ionospheric physics, density and composition of the upper atmosphere, remote sensing using atmospheric radiation; solar physics, infrared astronomy, infrared signature analysis; effects of solar activity, magnetic storms and nuclear explosions on the earth's atmosphere, ionosphere and magnetosphere; effects of electromagnetic and particulate radiations on space systems; space instrumentation; propellant chemistry, chemical dynamics, environmental chemistry, trace detection; atmospheric chemical reactions, atmospheric optics, light scattering, state-specific chemical reactions and radiative signatures of missile plumes, and sensor out-of-field-of-view rejection.